

AD-A086 469

ILLINOIS UNIV AT URBANA-CHAMPAIGN DEPT OF METALLURGY --ETC F/G 11/4  
STRUCTURE AND DEFORMATION CHARACTERISTICS OF RHEOCAST METALS.(U)  
MAR 80 R MEHRABIAN, F M HOSKING, F F PORTILLO DAAG46-76-C-0046

AMMRC-TR-80-5

NL

UNCLASSIFIED

1 OF 1  
AD  
AD-A086 469

END  
DATE  
FILMED  
18-80  
DTIC



12  
P.S.

AD

1741

ADA 086469

AMMRC TR 80-5

# STRUCTURE AND DEFORMATION CHARACTERISTICS OF RHEOCAST METALS

March, 1980

R. Mehrabian, F.M. Hosking, F.F. Portillo, R. Wunderlin

Department of Metallurgy and Mining Engineering  
Department of Mechanical and Industrial Engineering  
University of Illinois at Urbana-Champaign  
Urbana, IL 61801

DDC FILE COPY

FINAL REPORT

DAAG46-76-C-0046

Approved for public release; distribution unlimited.

DTIC  
ELECTE  
JUL 7 1980  
S A D

Prepared for

ARMY MATERIALS AND MECHANICS RESEARCH CENTER  
Watertown, Massachusetts 02172

80 7 3 095

The findings in this report are not to be construed as an official Department of the Army position, unless so designated by other authorized documents.

Mention of any trade names or manufacturers in this report shall not be construed as advertising nor as an official indorsement or approval of such products or companies by the United States Government.

#### DISPOSITION INSTRUCTIONS

Destroy this report when it is no longer needed.  
Do not return it to the originator.

UNCLASSIFIED

SECURITY CLASSIFICATION OF THIS PAGE (When Data Entered)

REPORT DOCUMENTATION PAGE		READ INSTRUCTIONS BEFORE COMPLETING FORM	
1. REPORT NUMBER AMMRC TR-80-5	2. GOVT ACCESSION NO. AD-A086 469	3. RECIPIENT'S CATALOG NUMBER 10018	
4. TITLE (and Subtitle) STRUCTURE AND DEFORMATION CHARACTERISTICS OF RHEOCAST METALS.		5. DATE OF REPORT & PERIOD COVERED Final Report, 24 June 76 to 23 June 79	
6. AUTHOR(s) R. Mehrabian, F. M. Hosking, F. Folgar, Portillo, R. Wunderlin		7. CONTRACT OR GRANT NUMBER(s) DAAG46-76-C-0046	
8. PERFORMING ORGANIZATION NAME AND ADDRESS Department of Metallurgy and Mining Engr. and Department of Mech. and Ind. Engineering University of Illinois, Urbana, IL 61801		9. PROGRAM ELEMENT, PROJECT, TASK AREA & WORK UNIT NUMBERS DA Project: 1T162105AH84 AMCMS Code: 62105A Agency Accession:	
10. CONTROLLING OFFICE NAME AND ADDRESS Army Materials and Mechanics Research Center Watertown, Massachusetts 02172		11. REPORT DATE March 1980	
12. MONITORING AGENCY NAME & ADDRESS (if different from Controlling Office)		13. NUMBER OF PAGES 195	
		14. SECURITY CLASS. (of this report) Unclassified	
		15. DECLASSIFICATION/DOWNGRADING SCHEDULE	
16. DISTRIBUTION STATEMENT (of this Report)  Approved for public release; distribution unlimited.			
17. DISTRIBUTION STATEMENT (of the abstract entered in Block 20, if different from Report)			
18. SUPPLEMENTARY NOTES			
19. KEY WORDS (Continue on reverse side if necessary and identify by block number) Metal matrix composites      Deformation Rheocasting                      Forging Solidification                    Thixoforging			
20. ABSTRACT (Continue on reverse side if necessary and identify by block number) This is the third and Final Report of a program initiated on June 24, 1976 to investigate the feasibility of producing net or near-net shape components of alloys and metal-matrix composites by forging type operations using Rheocast metals and composites. In two previous Interim Reports, we described the findings from the first two years of the program on: (1) The effect of process variables on the microstructure of a number of Rheocast alloys, (2) a comparison of the			

DD FORM 1473

1 JAN 73

EDITION OF 1 NOV 65 IS OBSOLETE

UNCLASSIFIED

SECURITY CLASSIFICATION OF THIS PAGE (When Data Entered)

1-6014

UNCLASSIFIED

SECURITY CLASSIFICATION OF THIS PAGE(When Data Entered)

Block No. 20

#### ABSTRACT

homogenization heat treatment response of Rheocast structures with conventionally cast dendrite structures of 2024 aluminum alloy, (3) the effect of pressure and die coatings on the heat transfer coefficient at the die-metal interface during forging of liquid and partially solid aluminum alloys, and (4) the Thixoforging of 2024 and 6061 aluminum alloy components, their microstructures and properties.

→ This Report describes work in the third and final year of the program aimed at developing wear resistant composites of aluminum base alloys, using Rheocasting and associated processes. It is anticipated that the feasibility of use of such composites in track blocks of land vehicles would be subsequently determined.

Composites of two wrought (2014 and 2024) and one cast (201) aluminum alloys containing 2 to 30 weight percent of  $Al_2O_3$  and SiC particles in the size range of  $1\mu m$  to  $142\mu m$  were prepared using a compositing apparatus developed in this investigation. The non-metals were successfully added and retained in the aluminum alloy matrices using the rheological properties of a partially solidified, vigorously agitated alloy to advantage. Subsequently, the composites were reheated to above their liquidus temperature, shaped and solidified under high pressure in a forging press.

The microstructures, the wear behavior and the mechanical properties of the composites were studied. Composites with particulate additions larger than  $5\mu m$  in size possessed homogeneous structures. On the other hand,  $1\mu m$  particles tended to cluster. The wear behavior of the composites was studied on a pin-on-disk type machine built during this investigation. It was shown that composites containing large amounts of non-metals, 20 wt%, of  $Al_2O_3$  or SiC exhibit excellent wear resistance and low coefficients of friction. The wear mechanism in the matrices and the composites were also established. It was shown that composites containing small to moderate amounts of non-metals possess tensile properties comparable to the matrix alloy, while increasing the amount of particulate additions results in reduced ductility. Finally, a method was investigated to produce components with high weight fractions of non-metals near their surface which would then possess both internal ductility and exceptional resistance to wear on their surface.

UNCLASSIFIED

SECURITY CLASSIFICATION OF THIS PAGE(When Data Entered)

## FOREWORD

Technical monitor of the contract was Mr. R. Gagne.

This research was supported by the Army Materials and Mechanics Research Center, Watertown, Massachusetts, under Contract No. DAAG46-76-C-0046. The 200 ton Autoforge press used in the pilot plant Thixoforging and composite forming system was donated by the Doehler-Jarvis Division of NL Industries, Inc.

Accession For	
DATE	
BY	
REMARKS	
DATE	

A

# TABLE OF CONTENTS

	Page
I. INTRODUCTION . . . . .	1
II. LITERATURE SURVEY . . . . .	2
A. Preparation and Mechanical Behavior of Metal Matrix Composites . . . . .	3
B. Wear Behavior . . . . .	10
III. APPARATUS AND PROCEDURE . . . . .	18
A. Fabrication of Composites . . . . .	18
B. Shape Forming of Composites . . . . .	21
C. High Volume Fraction and Dual Layered Composites . . . . .	22
D. Composite Compositions and Evaluation Techniques . . . . .	23
E. Wear Measurements . . . . .	24
IV. RESULTS AND DISCUSSION . . . . .	26
A. Microstructure of the Composites . . . . .	26
B. Mechanical Properties . . . . .	27
C. Fracture Surfaces . . . . .	32
. Friction and Wear Behavior . . . . .	33
V. CONCLUSIONS . . . . .	38
VI. REFERENCES . . . . .	40
TABLE I . . . . .	43
TABLE II . . . . .	44
TABLE III . . . . .	45
TABLE IV . . . . .	46
TABLE V . . . . .	47
TABLE VI . . . . .	48
TABLE VII. . . . .	49
FIGURES . . . . .	50

## I. INTRODUCTION

In the first two years of this program (1,2), a new net shape forming process, Thixoforging, was investigated. The process exploited the special structure and thixotropic rheological behavior of Rheocast metals to produce porosity free, heat treatable parts, in a single forming operation, thus eliminating the substantial manufacturing costs associated with machining operators. In the third and final year of this program, emphasis was shifted to research on aluminum matrix composites produced again using the rheological behavior of Rheocast matrices to advantage. The forging apparatus and techniques developed during the first two years were also used for the net-shape forming of the composites. Specifically, the investigation was concerned with the fabrication of aluminum alloy composites, the net shape forming of these composites, their microstructures, their friction and wear behavior and mechanical properties.

Composites of two wrought (2014 and 2024) and one cast (201) aluminum alloys containing 2 to 30 weight percent of  $Al_2O_3$  and SiC particles in the size range of  $1\mu m$  to  $142\mu m$  were prepared. The compositing apparatus developed in this investigation consists of a vacuum induction melting system, a controlled mixing assembly and a special vibration system for addition of the non-metals. The non-metallic particles were added to a partially solid, vigorously agitated matrix alloy. The particles were then retained in the matrix until interface interaction, probably the formation of  $Mg Al_2O_4$  spinel in the case of  $Al_2O_3$  particles



was facilitated. These composites were solidified and subsequently reheated to above their liquidus temperature and formed into shape under high pressure in a closed die forging type of apparatus.

The microstructures of the composites were studied using optical and scanning electron microscopy techniques. The wear behavior was studied on a pin-on-disk type machine built for this purpose. Finally, the tensile properties of the composites were determined.

## II. LITERATURE SURVEY

Increasing demand for lightweight, energy efficient materials in the government and transportation industries has stimulated increased activity in the materials community to develop specific alloys and processing techniques to meet this new challenge. It is anticipated that inexpensive light metal matrix composites may find a special demand if they meet specific friction and wear requirements while maintaining reasonable mechanical properties. The survey given below is divided into two general areas. First, available methods for the preparation of a variety of metal matrix composites are presented and the microstructures produced are related to mechanical properties. Second, a general description is given of our current understanding of wear mechanisms, and the effects of composition and process variables on the wear behavior of alloys containing particulate additions is discussed.

A. Preparation and Mechanical Behavior of Metal Matrix Composites

The wide range of properties that can be obtained in two-phase alloy systems with respect to single-phase metals has led to extensive research on these materials. Two-phase structures can be produced directly by controlled solidification, precipitation hardening and various dispersion hardening techniques (powder metallurgy and composite fabrication methods).

Much of the work done in this area deals with discontinuous second-phase particles that are uniformly distributed in an alloy matrix. Oxides, carbides, silicides, borides and other non-metallic dispersoid systems have shown some degree of promise in wear and strengthening applications.

An important group of these hard, second-phase particles consists of those that are insoluble in the matrix and are stable at high temperatures. Oxides, carbides and nitrides are generally considered in these studies. Another classification of dispersoids involves those where the second phase can react with or dissolve in the matrix. These structures are generally based on intermetallic compounds produced from solidification or solid state transformations. The dispersoid is usually softer and unstable at higher temperatures.

There are a number of techniques available for the production of various dispersed phase alloys. They include solid state transformations, liquid-liquid reactions, liquid-solid reactions, gas-liquid reactions, gas-solid reactions and mechanical mixing. Gas-solid reactions [3,4] comprise some of the most promising

methods for producing the finest oxide dispersions ( $\ll 1\mu$ ) obtainable in current practice. Specific examples of the gas-solid reaction include surface oxidation, internal oxidation and a combination of the two methods.

Surface oxidation [3] is used in the fabrication of SAP-type alloys. Metallic powders with a very high specific surface area have their surfaces oxidized. This is followed by compaction, sintering and hot extrusion that breaks up and disperses the oxide film. A volume percent from 12 to 14 of the oxide phase can be obtained that is relatively uniform and reproducible.

Internal oxidation [4] involves the formation of stable oxide particles in a dilute solid solution where the solute is more active than the solvent. The size of the oxide particle is related to the absolute free energy of formation of the oxide, temperature of oxidation, solute content and effective depth of internal oxidation. A good dispersion by this method will require the oxygen to diffuse much faster than the solute in the matrix. The thickness of the section that can be processed is an important limitation to this technique.

Surface plus internal oxidation [4] combines the above two techniques using metal powders to overcome the restrictions on the obtainable size of the specimen. There is a significant conversion of solute to fine refractory oxide particles. The less stable oxides are eliminated by further selective reduction.

Mechanical mixing [5] is very versatile and adaptable to many alloy-dispersoid systems. It requires the blending of alloyed powders with fine oxide particles. Compaction, sintering and

extrusion follows the blending. Generally, an oxide content of 0.5 to 15 volume percent is added giving a series of fine particle dispersions of increasing strength and decreasing ductility with increasing oxide content. Limitations encountered involve obtainable particle size and segregation of the oxide particles.

A promising technique that does not require powder metallurgy methods involves the preparation of a composite with the desired dispersed second phase in a metal alloy matrix [6,7]. The process involves taking advantage of the rheological behavior and structure of a partially solidified, agitated matrix alloy. The hard non-metallic particles are added to and retained as a relatively homogeneous dispersion in the partially solid alloy mixture. This agitated slurry prevents floating, settling or agglomeration of the particles and allows wetting between the particles and liquid matrix of the slurry. A limitation of this method includes the difficulty of adding very fine particle sizes without clustering or segregation prior to addition and within the metal matrix. For fine to moderate size particles ( $3\mu$ - $150\mu$ ), however, the technique permits the fabrication of materials that exhibit improved friction and wear behavior while maintaining reasonable engineering strength. An important factor, in addition to improved friction and wear properties, leading to the development of such composites is the consideration of material selection versus product economics. It becomes very practical to replace a more expensive material by a less expensive alloy containing a dispersoid that maintains the same mechanical design requirements.

The properties of dispersed phase alloys are dependent on

several characteristics of the dispersion. The effects of these variables are complex and there are disagreements regarding which parameters contribute the most. This stems primarily from differences in the systems examined. Parameters influencing the mechanical behavior include volume fraction of the particle, particle size and spacing, particle morphology, hardness and strength of the particle versus the alloy matrix, degree of bonding of the system, stored energy from the mechanical working, recrystallization temperature, and fracture characteristics (crack nucleation and propagation).

Studies made to evaluate the properties and behavior of dispersed phase alloys can be divided into three groups. The first group consists of those particles with sizes greater than one micron. The next group deals with pre-precipitation phenomena of solid state transformations. The final group pertains to small, inert dispersoids much smaller than one micron. The variables controlling properties and the deformation and the strengthening mechanisms seem to be different in every case. The first group of dispersions will be considered in this review.

Edelson and Baldwin's investigation [8] on dispersion-strengthened copper alloys considered the behavior of dispersions of particles larger than one micron in size. Powder metallurgy techniques were used to fabricate alloys consisting of dispersions of chromium, iron, alumina, molybdenum, graphite, lead and voids in copper. Particles ranging in size from 5 to 200 $\mu$ , volume fractions of 0-0.25, mean free paths of 25-45 $\mu$ , and interparticle spacings of 5-8 $\mu$  were tested.

The volume fraction ( $g$ ) and particle size ( $d$ ) of the discontinuous second phase were taken as independent variables. From these two variables, the mean free path ( $\lambda$ ) and interparticle spacing ( $D_s$ ) were determined using statistical analysis resulting in the following relationships:

$$g = \frac{WD_1}{(1-W)D_2 + WD_1} = \text{Volume Fraction} \quad (1)$$

where  $W$  = weight fraction dispersoid

$D_1$  = density of matrix

$D_2$  = density of dispersoid

$$\lambda = \frac{2}{3} \frac{d}{g} (1-g) \quad (2)$$

$$D_s = d (1-g) \sqrt{2/3g} \quad (3)$$

The mean free path was taken to be the distance moved from a given reference particle to a second particle that is taken as an average in all directions. Interparticle spacing may be thought of as the average diameter of space-filling cells centered on the dispersoid particles. This is schematically shown in Figure 1 [8]. The relationships between  $g$ ,  $d$ ,  $D_s$  and  $\lambda$  are illustrated in Figure 2 using the equations given above.

It was shown that iron and chromium particles increased the yield strength. The voids, alumina, graphite, lead and molybdenum dispersions showed no improvement. In all cases, strengthening occurred when a strong particle-matrix bond was formed. The strong bond allowed for a boundary between the particle and matrix

capable of supporting the local strain field developed under load. When strengthening does occur, the yield stress was shown to be a function of the mean free path (that is, particle size and volume fraction). Hardening seems to fall off above a critical mean free path whose value varies directly with the particle diameter as shown in Figure 3 [8].

Ductility, as measured by reduction in area, is a function of volume fraction and is independent of particle size. The general trend as shown in a plot of ductility versus volume fraction in Figure 4 [8] shows the effect of second phase additions as always being embrittling regardless of their effects on strengthening. The second phase, especially those with irregular shapes, act as areas where crack initiation and propagation may occur as a result of local stress concentrations. This causes the metal to reach its fracture strain at much lower overall strain. It should be noted that the strain hardening exponent and fracture stress follow the same general behavior as the ductility.

Mogford [9] gives a good review of deformation and fracture of dispersed second phases in alloys. The yield stress of the dispersion strengthened alloy should generally be greater than that of the matrix by itself and this effect is a result of the hard, rigid particles exerting constraint on the matrix.

The most significant role of these particles is to lower the ductility of the matrix alloy as a result of failure at the weakest interface. The strength is therefore dependent on particle-matrix bonding and independent of the type of hard particles used. Particles that have weak bonds with the matrix act as sites

for failure by decohesion and void nucleation.

Levi, et al [10] examined the interface interactions of alumina fiber (3-6mm long) with aluminum alloys. Composites of homogeneous dispersions of  $\text{Al}_2\text{O}_3$  fibers were obtained by adding them to agitated, partially-solid slurries of Al-Mg, Al-Cu and Al-Cu-Mg alloys. The fibers appeared wetted and bonded to the matrix.

Microscopic examination of the composites revealed the existence of an altered microstructure around the  $\text{Al}_2\text{O}_3$  fibers which consists of a fine multiphase material. Features common to all the structures were the existence of an intimate bond, the absence of voids at the fiber boundary and the presence of fine polycrystalline  $\alpha\text{-Al}_2\text{O}_3$  in the interaction zone. The average maximum thickness of this "apparent interaction zone" depends on residence time and alloy composition as shown in Figure 5 [10]. Residence time was taken as the time the fiber was in contact with the agitated, partially-solid slurries after addition plus the time for remelting and solidification.

In the case of Al-Mg alloys, bonding was achieved through formation of a  $\text{MgAl}_2\text{O}_4$  (spinel) layer by reaction between the fiber and the Mg in the liquid Al. The Al-Cu-Mg alloys were observed to have  $\text{MgAl}_2\text{O}_4$ ,  $\alpha\text{-Al}_2\text{O}_3$  and possibly  $\text{CuAl}_2\text{O}_4$  coexisting in the interaction zone.

Levi, et al [10] postulated that a compound of the aluminate type was formed on the fiber surface and provided the necessary bond with the surrounding matrix. Examination of fracture surfaces of the composite revealed that in general, the failure was not at the interface, but rather by plastic flow at the matrix around the fibers.



In conclusion, the properties of coarse particle dispersions, which is of interest to the present investigation, seem to be dependent on the geometric variables of dispersion (e.g. the mean free path ( $\lambda$ )) and the structural characteristics of the dispersoid (e.g. strength and bond formation).

There are several techniques available for the production of dispersed phase alloys. Most of them are adaptable to only particular applications, and clustering or segregation of the dispersions are an important problem to overcome. Powder metallurgy methods are used in most of the techniques to produce fine dispersions. For coarser dispersions, the composite fabrication process described in this investigation provides an alternate approach that should lend itself to production of the composites continuously and economically.

#### B. Wear Behavior

Wear is generally defined as the unwanted removal of material by chemical or mechanical action. Wear classifications can depend on the wear rate, wear mechanism, the type of relative motion etc. For example, the amount of material lost could be used to define mild or severe wear. On the other hand, Czichos's [11] classification of the types of wear, shown in Table I, is based on the type of relative motion and wear mechanism. He states that in order to specify the type of wear it is necessary to take into account:

- i. type of relative motion
- ii. dominant wear mechanism
- iii. material properties relevant to wear
- iv. wear rate, and
- v. appearance of the worn surface.

Abrasive wear mechanism usually develops when one of the surfaces, in contact and in relative motion, is much harder than the other. Grinding of a piece of metal by the hard particles on an emery paper or the asperities of a harder surface are examples of such wear.

In what follows, first the different wear mechanisms are reviewed and some experimental data between wear rate and process variables are presented. Second, transition between mild and severe wear which is characteristic of dry sliding wear of metal rubbing against metals is discussed. Finally, some experimental results of aluminum alloys under dry sliding wear are presented which show the effects of composition and process variables on the wear processes in these alloys.

#### Wear Mechanisms

There are five basic wear mechanisms:

- i. abrasive wear
- ii. adhesive wear
- iii. surface fatigue wear
- iv. erosion wear, and
- v. corrosive wear.

Since in most instances two or more wear mechanisms may be operating concurrently, the dominant wear mechanism is established by analysis of the worn surface under the microscope. It is also important to remember that the type of relative motion plays an important role in the wear mechanism. Finally, the dominant wear mechanisms may change due to changes in the test conditions. For example, a transition from mild to severe wear may result from an increase in load and/or sliding velocity.

Kruschov [12] has defined the abrasive wear resistance ( $\epsilon$ ) as the inverse of the measured wear volume:

$$\text{wear resistance } \epsilon = \frac{1}{V_{\text{wear}}} \quad (4)$$

The wear volume in abrasive wear has been found to be proportional to the applied load and the sliding distance. Experimental results also show an inverse linear relationship between wear volume and hardness - this is especially true for cast irons [13].

Adhesive wear mechanism is developed when the applied pressure is large enough to produce local plastic deformation which eventually results in metal transfer by adhesion of the asperities of one surface to the other. Therefore, surface properties of metals, rather than bulk properties, play a prominent role in this wear mechanism. Wear tests in vacuum have shown that adhesive wear can be induced between almost any pair of metallic surfaces and that adhesion bonding is enhanced by mutual solubility of the metals in contact. Furthermore, this type of wear is also influenced by crystal structure, crystal orientation and small alloying additions in some metallic systems [11].

Surface fatigue wear mechanism is ascribed to continuous stress cycling in rolling contact. Suh [14] has attempted to explain the formation of sheet-like wear particles by taking into account the stress field beneath the surface of contact and a dislocation interaction model. However, a fatigue limit stress for this type of wear has yet to be found for design purposes of infinite life conditions.

Erosion wear and corrosive wear are not of direct interest to this investigation. The former wear mode occurs where particles flowing in a fluid stream strike a surface, while the latter is generally due to operative corrosion mechanisms such as the acid condition of a lubricant.

#### Effect of Variables on Sliding Wear

The important variables affecting sliding wear have been demonstrated to be:

- i. Sliding distance
- ii. Contact interface: Contact area, shape, finish and atmosphere
- iii. Load and Velocity
- iv. Material properties.

One of the first relationships between process variable and wear volume was that proposed by Archard [15]. It is:

$$V = K \frac{PL}{3H} \quad (5)$$

where  $V$  = wear volume,  $P$  = load,  $L$  = sliding distance,  $H$  is the hardness of the softer material and  $K$  is a proportionality constant.

Since then, most of the work which has made use of equation (5), has been directed toward finding correlations between the proportionality constant  $K$  and various material and test variables.

Under abrasive conditions, wear volume is usually found to be proportional to the sliding distance. However, exceptions are noted for the case of dry metal to metal sliding wear. For example, Bhansali [16] has reported that cobalt and nickel base alloys display

variable and sometimes abrupt changes in wear rate with sliding distance. He has postulated that wear rate is influenced by changes in microstructure such as the exposure of carbides in a cobalt-base alloy subsequent to wear of the surrounding matrix.

Wear data obtained is influenced by the geometry of the device, the contact interface and the atmosphere in important ways. For example, in the case of a pin-on-disc machine the wear rate of the specimen will depend on whether it is used as the pin or the disc. This is due to the fact that the pin is always in contact with the disc whereas the surface of the disc goes in and out of contact as it rotates, producing different temperature distributions on the pin and on the disc. Variations in the specimen temperature can be responsible for phase changes as well as oxidation. The former has been observed by Hogmark et al [17] on several martensitic steels. On the other hand, the atmosphere surrounding the contact interface also plays an important role when oxide formation becomes the dominant wear process.

As noted in equation (5) the wear rate under dry sliding conditions increases with increasing applied normal load. However, changes in the microstructure and the microchemistry of an alloy can affect this finding. For example, Bhansali [16] reports that the presence of oxides in nickel-base alloys and carbides in cobalt base alloys result in anomalous behavior in the wear rate as a function of applied load.

The effect of sliding velocity on wear rate is not well defined because it can influence the operating wear mechanism itself. Quinn et al [18] have proposed an equation in which the wear rate is

inversely proportional to the sliding velocity. However, application of this type of relationship to materials such as steels is questionable. Hogmark et al [17] working with martensitic steels found that at low sliding velocity the dominant wear mechanism was corrosive. At high sliding velocity and high loads the wear was severe due to the high contact temperature produced by the adhesive wear mechanism. Bhansali [16] postulated a shift in the wear mechanism of nickel base alloys from mild to severe wear at higher sliding velocities at low applied loads.

Mild to severe transition in dry sliding wear has been the subject of a number of studies [19-21]. It is generally agreed that increasing the hardness of the contact surface pushes this transition to higher loads. For example, Arnell et al [20] report that mild-severe transition occurs when the maximum shear stress in the region of contact reaches one-sixth of the material hardness. While this simple correlation was deduced from a number of experiments on copper, brass and mild steel against a hardened steel disc, it is unlikely that it would hold for other materials and test conditions.

The presence of discrete hard or soft particles in a matrix can influence wear behavior in important ways. Both Hogmark et al [17] and Sato et al [22] found reduced wear when the matrix alloy contained hard particles. The presence of soft particles could increase wear rate [22,23]. However, this observation may have been due to the poor bonding between the particles and the matrix [23].

### Wear of Aluminum Alloys

Most of the research and development efforts have been directed toward applications where the bearing properties of aluminum alloys are of primary importance. Examples of these applications include the use of aluminum-tin alloys where optimum boundary lubrication is required and aluminum-silicon alloys in the internal combustion engine as cylinder blocks, cylinder heads and pistons.

Aluminum alloys display two basic wear mechanisms, oxidative or mild wear and metallic or severe wear. The onset of severe wear is taken as the start of seizure and the sliding distance that corresponds to this point is designated as the "point of seizure". Most studies of dry sliding wear have been concerned with the effects of applied load, sliding velocity and alloy composition on seizure resistance. For example, it has been found that additions of copper to aluminum improve the seizure resistance, particularly at higher sliding velocities [24]. On the other hand, applied load and to a lesser extent, sliding velocity influence the point at which seizure occurs, but have no effect on the mechanism of seizure.

Additions of silicon, especially in the hypereutectic composition range which results in formation of primary hard silicon particles in the matrix, improves the wear resistance of aluminum alloys. Shivanath et al [25] have shown a continuous increase in the transition load with increasing silicon content in this composition range. However, oxidative wear rates (mild wear) appears to be independent of both silicon content and the particle size of the silicon. Mild wear rate  $q$  (g/cm) in aluminum alloys has been

correlated to the applied load  $P(g)$  by the following equation [26]:

$$q = KP^\alpha \quad (6)$$

where  $\alpha \approx 0.4$  to  $0.6$

and  $K$  is a proportionality constant which depends on the material being tested.

The mild and severe wear regimes of aluminum-silicon alloys have been distinguished by both the magnitude of the volume wear rate and the operating mechanisms [25]:

Oxidative wear rate:  $10^{-8}$  to  $10^{-7}$   $\text{cm}^3/\text{cm}$

Metallic wear rate:  $10^{-5}$  to  $10^{-4}$   $\text{cm}^3/\text{cm}$

Finally, in one oxidative (mild wear) experiment transfer of iron from the steel disc to the wear pin surface has been reported [25]. It is postulated that the protective surface film contains a uniform high distribution of Al/Fe intermetallic. On the other hand, metallic or severe wear is characterized by plastic deformation and shear with a roughened surface appearance when viewed in the SEM [25].



### III. APPARATUS AND PROCEDURE

Aluminum matrix composites of two wrought alloys 2014 and 2024 and one cast alloy 201 containing particulate additions of  $Al_2O_3$  and SiC were produced in a vacuum induction melting and casting system especially modified for this purpose. The composite fabrication technique is based on that previously described by Sato et al [22]. The composites were subsequently reheated to above their liquidus temperature in a second induction furnace and forged into shape in a 200 ton hydraulic press. The microstructures of the composites were studied and their tensile properties were determined. Finally, disc shaped wear test specimens were removed from the forged composites and their wear behavior was studied on a pin-on-disk type machine designed and constructed in this investigation.

#### A. Fabrication of the Composites

Photographs and a schematic illustration of the modified vacuum induction system used to fabricate the composites are shown in Figures 6 and 7. The apparatus consists of an induction power supply (50KW, 3000 cycles) a water-cooled vacuum chamber with its associated mechanical and diffusion pumps, and a crucible and mixing assembly for agitation of the aluminum alloy melts prior to and during the preparation of the composites. The composite

fabrication procedure included partial solidification of an aluminum melt in vacuum while it was subjected to vigorous agitation. The non-metallic particles were then added to the partially solid alloy slurry while agitation was continued. The non-metals were thus entrapped in the melt while interaction between the particles and the matrix promoted wetting (22).

The vacuum induction furnace shown in Figures 6 and 7 has several ports for observation of the melt and the incorporation of water, gas and electrical feedthroughs. The mixing assembly located on top of the furnace is co-axially aligned through an O-ring seal at the top of the chamber and a bearing block just above the crucible.

The blades are made of cast iron that were sand cast and ground with a curved taper. The overall blade dimensions are 76mm long, ~ 40mm high and ~ 40mm wide at the center with a taper down to 6mm at the blade tip. Two blades were utilized mounting one perpendicular to the other on the shaft. A protective refractory coating of Sauereisen paste (No. 1) was applied to the blades to prevent interaction with the molten melt. This was further coated with a carbon wash. A conical graphite plug (~ 40mm diameter by ~ 40mm) was screwed on at the base of the shaft below the two blades to complete the assembly.

An aluminum crucible (~ 90mm diameter by ~ 150mm) with a bottom hole was designed and used in the furnace. A tapered graphite insert with a center hole (25mm diameter) was positioned at the bottom of the crucible to allow bottom pouring of the composite. The graphite plug on the blade assembly mates with this insert

during the preparation of the composite. This rotating seal prevents leakage of the melt. The charge capacity of the furnace is approximately 1 kilogram for an aluminum alloy with the blade assembly in position.

The composites are cast in a water-cooled graphite mold,  $\sim 90\text{mm}$  in diameter by  $\sim 125\text{mm}$  high, located directly below the crucible assembly. The non-metallic particles are introduced into the alloy slurries by means of a magnetic feeder device with a variable controller to regulate the feed rate. The trough is positioned such that the particles enter the melt between the rotor and the crucible wall.

Approximately one kilogram of aluminum alloy was placed in the system with the blade assembly in place. The chamber was pumped down to 0.15 torr pressure using the mechanical pumps only. The alloy was superheated above its melting temperature and the agitation was initiated as noted above. The induction power was gradually lowered until the alloy was 40 to 50 percent solid at which time the non-metallic particulates were added to the slurry. The power input was controlled such that the total percent solid, non-metals and solid spheroids of the alloy, did not exceed  $\sim 50$  percent. Rotation speed of the blade was generally maintained at 240 RPM. Stirring was continued until interface interactions between the particulates and the matrix promoted wetting (27). The melt was then superheated to above its liquidus temperature and bottom poured into the graphite mold by raising the blade assembly.

## B. Shape Forming of the Composites

The forging apparatus used is shown in Figures 8 and 9. It consists of a high frequency induction furnace and power supply (400V, 15KW, 3000 cycle) and an automated hydraulic (200 ton) forging press modified to permit shaping and solidification of completely liquid and partially solid charge materials under pressure [2].

The forging dies illustrated in Figure 10 were sprayed with a thin coating of graphite powder mixed with isopropyl alcohol. A ring insert was placed in the lower die half to allow fabrication of shapes that would provide material for wear and mechanical testing. The smaller diameter ( $\sim 80\text{mm}$ ) section was used to study the wear properties and the larger diameter ( $\sim 115\text{mm}$ ) section was used to examine the mechanical properties of the composites.

The shape forming sequence of operations were as follows. The cast composites were placed in an alumina crucible ( $\sim 100\text{mm}$  in diameter by  $170\text{mm}$  high) and reheated in the induction furnace to a superheat of  $50\text{K}$ . The temperature was closely monitored with a thermocouple to prevent overheating. The crucible was then removed from the furnace. The oxide film on top of the melt was skimmed off, and the melt was gently stirred mechanically to avoid particle settling. The melt containing the non-metallic particles was then transferred into the lower die half of the press and the top die was brought down to shape and solidify the composite under an applied pressure of approximately  $2 \times 10^8$  Pascals. The pressure was maintained for 90 seconds to complete the solidification before the composite was ejected. Solidification in the unheated steel dies

under direct applied pressure resulted in a structure free of macroporosity with a relatively homogeneous distribution of the non-metallic particles. Figure 9(b) shows a representative shaped composite part produced in this investigation.

### C. High Volume Fraction and Dual Layered Composites

In certain applications it may be desirable to have a composite with high volume fraction of non-metals ( $\sim 0.5$ ) or one with a gradation of non-metallic particulates - e.g. a wear resistance surface backed by a ductile matrix. Two similar but slightly different techniques were developed for the production of such composites.

In the first process a porous ceramic filter was used to remove a portion of the matrix liquid during the forming operation. This 20 mm thick ceramic filter, a product of Consolidated Aluminum called Selee, was first located in the bottom of the lower die. A 3mm thick layer of 150 $\mu$ m size  $Al_2O_3$  particles was spread uniformly on the top of the filter. This was done to prevent infiltration of particles on the composite into the porous filter. The composite was superheated to 50K above its liquidus temperature, transferred to the lower die half and solidified under pressure as previously described. Figure 11 shows a schematic illustration of the experimental set-up prior to and after the forming operation. This process was successful in producing high volume fraction composites. It should be noted that a thin layer of matrix  $\sim 2$  to 3mm thick, devoid of non-metallic particulates, was consistently noted at the top of the composites following this operation.

Composites with a variable concentration of non-metallic particles were readily produced using a second technique. The procedure followed was to sequentially add the composite and a superheated liquid melt devoid of any particles into the lower die half prior to pressurization. The viscous composite, ~ 6.0mm thick, remains at the bottom of the disc-shaped part if the matrix alloy is added gently by means of a coated stainless steel trough. Composite parts produced in this way contain a sharp discontinuous non-metallic composition gradient.

#### D. Composite Compositions and Evaluation Techniques

Composites of two wrought and one cast aluminum base alloys were prepared. Table II gives a list of the composites fabricated. The nominal compositions of the matrix alloys studied were:

- (a) 2014 - 4.4% Cu, 0.8% Si, 0.8% Mn, 0.4% Mg, BALANCE Al
- (b) 2024 - 4.5% Cu, 1.5% Mg, 0.6% Mn, BALANCE Al
- (c) 201 - 4.7% Cu, 0.39% Mg, 0.3% Mn, 0.6% Ag, 0.2% Ti,  
BALANCE Al

The disc-shaped parts, Figure 12, were sectioned with a diamond saw to prepare specimens for friction and wear and mechanical behavior studies. The friction and wear properties were investigated on a pin-on-disc type machine.

Standard round tensile specimens of 6.35mm gage diameter and 25.4mm gage length were tested with an Instron testing machine at a strain rate of 1.25mm per minute. The solutionizing and aging parameters of the alloys used are listed in Table III.

Elevated temperature tensile tests were also performed with the same specimen dimensions as used in the room temperature tests. An MTS mechanical testing system with a high temperature furnace (1275K max.) mounted on the load frame was utilized. The tensile specimens were heated up to a temperature of 525K and held at this temperature for 15 minutes to allow for a uniform temperature distribution throughout the specimen. Testing proceeded subsequently at a stroke rate of 1.0 mm/min.

#### E. Wear Measurements

The friction and wear measurements were carried out on the pin-on-disk type machine shown in Figures 13 and 14 which was especially built for this investigation. It is similar to the machine described by Burwell and Stange [28] and Wu [29].

The circular disc with the specimen holders is driven by a 1/8 HP variable speed DC motor coupled to a 10 to 1 ratio worm gear reducer. The speed of the motor was varied on different wear track diameters such that a constant speed of 10 cm/s could be maintained throughout all the tests. The normal force is imparted by placing weights on the rider (pin) which is attached to the end of the counter-weighted flexible arm shown in Figures 13 and 14. An aluminum dynamometer ring ~ 9cm in diameter by ~ 2cm wide and ~ 0.12cm thick with strain gages attached on the inside and outside of the ring is used to measure the bending strain due to the friction force. The signal, which is obtained through a differential amplifier, is recorded on a Gould strip chart recorder. The average coefficient of friction is then calculated from this data.

The rider (pin) consists of a vertical treaded ( $\sim 6.3\text{mm}$  diameter) rod which fits at one extremity of the dynamometer ring. A  $6.4\text{mm}$  diameter AISI type E-52100 ball bearing\* was attached to the end of the pin with epoxy. A new ball bearing was used at the beginning of each test.

The composite specimens,  $\sim 80\text{mm}$  in diameter by 2 to  $4\text{mm}$  thick were removed from the smaller section of the shaped forging shown in Figure 12. Two disc-shaped specimens were removed with a diamond saw from each forging. These were machined flat and polished with 600 grit SiC paper prior to each test. All the specimens were tested in the as-cast condition with no heat treatment.

The wear test consisted of weight loss and coefficient of sliding friction measurements on the matrix alloy and composite specimens sliding against the ball bearings noted above. All tests were carried out under dry sliding conditions. Prior to each test both the disc and the bearing were degreased with acetone. The weight loss was measured with an accuracy of  $\pm 0.1\text{mg}$  after every 100 meters of sliding.

Wear mechanisms were studied by examination of specimens polished with  $6\mu\text{m}$  diamond compound followed by  $0.3\mu\text{m}$   $\text{Al}_2\text{O}_3$  particles prior to each test. The wear tests were run from a few cycles up to 2000 meters. The tracks were examined with optical and scanning electron microscopes.

---

\* The Anti-Friction Bearing Manufacturer's Association grade of the ball bearing used is 25.



#### IV. RESULTS AND DISCUSSION

The disc-shaped composites produced were sectioned, their structures were examined by Scanning Electron Microscope techniques and their mechanical, friction and wear properties were determined.

Table II lists the various composites produced and shaped in this investigation. As previously noted, two wrought and one casting alloy were used as matrices. The non-metallic additions,  $\text{Al}_2\text{O}_3$  and  $\text{SiC}$  particles in the size range of 1 to  $142\mu\text{m}$ , were made to the partially solid alloy matrices. Weight percent of the particles added was varied from 2 to 30 percent. Results of the microstructural evaluation of the composites, their tensile properties at room temperature and at 525K and their behavior are discussed below.

##### A. Microstructure of the Composites

Representative microstructures of the liquid forged, disc-shaped composites are shown in Figures 15-19. A high weight percent addition of coarse  $\text{Al}_2\text{O}_3$  particles generally resulted in homogeneous distributions of the non-metals in the aluminum alloy matrices. Note the uniform distribution of the particles in Figures 16-18 as well as the absence of voids in the surrounding matrix. The latter is attributed to solidification under the high direct applied pressure in the forging press. Relatively uniform distributions were observed in almost all the composites produced when the weight percent and size of the non-metallic additions were 5 percent or more and  $5\mu\text{m}$  or larger, respectively.

Representative microstructures of different matrices containing 5 weight percent of  $\text{Al}_2\text{O}_3$  are shown in Figures 15-19(a).

On the other hand, significant particle clustering (formation of segregated regions of concentrated particles surrounded by regions of matrix devoid of particles) was observed when the particle additions were in the  $1\mu\text{m}$  size range, Figure 19(b). Attempts to break-up these clusters by mild mechanical agitation of the remelted composites, prior to forging, were not successful. Severe agitation was avoided because it causes air entrapment in the composite. It is postulated that the clusters form during composite fabrication, when the fine particulates are added to the alloy slurry, and are entrapped in the liquid matrix surrounding the primary solid particles. Agitation of the reheated composites prior to forging, while not effective in breaking up the clusters, did insure a uniform distribution of the clusters themselves in the shaped part.

Interface interactions between  $\text{Al}_2\text{O}_3$  and aluminum matrices during fabrication of composites using mechanical agitation have been previously investigated (10,32). The formation of an  $\text{MgAl}_2\text{O}_4$  and  $\text{CuAl}_2\text{O}_4$  spinels and other interactions (10) between alumina fibers and aluminum matrices has already been discussed. Close examination of these interfaces using Auger and electron diffraction techniques (32) has verified the earlier findings. Particulate composites produced in the present investigation revealed

excellent intimate bonds between the  $\text{Al}_2\text{O}_3$  particles and the various matrices. All three matrices contain magnesium and copper as alloy element additions. Thus, it is postulated that interactions similar to those noted above are responsible for bonding at the interfaces.

Figure 20 shows optical microscope views of a dual layered, high volume fraction composites of a 2024 aluminum alloy made using the special ceramic filter and oxide particles shown in Figure 11. The oxide particles,  $142\mu\text{m}$  in size, were identical to those put in the alloy matrix. These were sprinkled on top of the filter in order to prevent the particles in the composite itself from infiltrating the ceramic filter. Thus, the lower extremity of the structure shown in Figure 20 consists of infiltrated  $\text{Al}_2\text{O}_3$  particles which are not completely wetted by the matrix alloy. This oxide layer was separated from the dual layered composite by means of a diamond saw. Thus, the final product was a disc-shaped part composed of two layers, a 2024 alloy matrix followed by a composite containing approximately 30 weight percent of  $142\text{ m}$  size  $\text{Al}_2\text{O}_3$  particles. It is postulated that composites thus produced would be used in applications where exceptional wear properties on a given surface are desired in combination with a relatively ductile internal microstructure.

Other techniques, such as the dual layered technique described in the procedure, are equally successful in producing tailored inhomogeneous composites such as the one discussed above. In the latter approach introduction of the superheated matrix alloy on top of the remelted composite had to be carefully controlled to avoid

intermixing of the two. Dual layer composites like the one in Figure 20(b) were successfully produced in this way.

Finally, other processing options such as centrifuging during solidification of an axisymmetric part can be used to effectively segregate heavy or light non-metallic additions to the outside and inside extremities of the part prior to solidification. Gravity segregation of particles in a composite during slow solidification in a heated mold is a further processing technique that can be utilized for the production of such composites.

#### B. Mechanical Properties

The main objective in the production of the aluminum matrix composites and their subsequent shape forming is for use as net or near net shaped components in applications requiring exceptional wear behavior. However, it is essential that such composite components, or surfaces in the case of intentionally segregated composites, possess predictable minimum acceptable mechanical properties. The room and high temperature tensile properties of the composites reported below were determined to satisfy the latter requirement.

The disc-shaped composites were sectioned with a diamond saw into rectangular blanks for subsequent machining of the tensile test bars shown in Figure 12. All the composite specimens and the

matrix alloys shaped in an identical manner were tensile tested in the heat treated T-4 condition. The control samples of the matrix alloys were also heat treated to a T-6 condition and tested for comparison with data available in the literature, specimens pulled from the wrought alloys used in this study and data from previous work on squeeze cast (liquid forged) and Thixoforged disc-shaped parts [2]. Table III lists the various time and temperature of the heat treatments, while Table IV lists the commercial room temperature properties reported in the literature and those determined in an earlier investigation on the same forging press [2].

Average room temperature tensile properties of the composites and the matrix alloys in the T-4 condition determined in this investigation are listed in Table V. The tensile properties of the matrix alloys in the T-6 condition are listed in Table VI. The latter should be compared to those in Table IV as well as the ones shown from an earlier study [2] on Squeeze Casting (liquid forging) and Thixoforging (forging of Rheocast alloys). Several observations are readily made by comparing the data in Tables IV to VI.

First, the better properties, ductilities, of the earlier study [2] are attributed to the fact that the alloys were degassed and protected with nitrogen prior to the forging operation. Oxide entrapment was thus minimized in these forgings. Second, the higher volume fraction composites were very brittle and possessed low tensile properties. For example, the 20 weight percent composites in the T-4 condition had an average tensile strength of 16.5 Kg/mm<sup>2</sup> and a corresponding elongation of approximately 0.4. The low ductilities in these specimens can be attributed to the large

number of blocky particles with sharp corners which make the composites prone to localized crack initiation and propagation. Third, the lower volume fraction composites containing relatively homogeneous distributions of fine  $\text{Al}_2\text{O}_3$  retain reasonable tensile properties comparable to and in some cases exceeding the yield strength of the matrix alloy solidified under identical conditions. For example, note the tensile data on 2014 and 201 alloy composites containing 5 weight percent of  $5\mu\text{m}$  size  $\text{Al}_2\text{O}_3$  particles. These latter observations are in line with those reported by Sato et al. [7] for hot extruded composites of aluminum alloys prepared in a similar manner.

Results of the Edelson and Baldwin [8] reviewed earlier and reported in Figure 4 show that ductility, as measured by  $\ln(A_0/A_f)$ , continuously decreases with increasing volume fraction of particulate additions and appears to be independent of particle size. The data in Table V are plotted in a similar manner in Figure 21. The volume fraction of the  $\text{Al}_2\text{O}_3$  particles in the composite was determined from the data in Table V and the following equation:

$$g = \frac{WD_1}{(1-W)D_2 + WD_1} = \text{volume fraction} \quad (1)$$

where,

$W$  = weight fraction charged

$D_2$  = particle density  $\sim 3.72 \text{ g/cc}$  [ $\text{Al}_2\text{O}_3$ ]

$D_1$  = matrix density  $\sim 2.8 \text{ g/cc}$  [for 2014, 2024]  
and  $\sim 3.0 \text{ g/cc}$  [for 201]

The trend established between ductility and volume fraction of  $Al_2O_3$  is similar to that reported earlier [8]. However, the ductilities of the present study appear to fall far lower than Edelson and Baldwin's curve [8] also shown in this figure. It is postulated that their higher ductilities can be attributed to the very ductile, forgiving copper matrix used.

The measured elevated temperature, 525K, tensile properties of the matrix alloys and the composites are listed in Table VII.

The higher volume fraction specimens were not tested due to their poor room temperature tensile properties. Small improvements in the elongation were observed with ultimate strength values decreasing anywhere from 8-15  $Kg/mm^2$ .

### C. Fracture Surfaces

The fracture surfaces of the tensile specimens were examined in order to determine the nature of failure of the composites. Figure 22 shows typical Scanning Electron Microscope fractographs of two fracture surfaces of the composites tested at room temperature. The particles show little or no signs of cracking and appear to be well bonded to the matrix. Failure of the composites seems to have occurred through the matrix as a result of void coalescence as exhibited by the "dimpled" regions in the matrix. It is believed that the sharp morphology of the alumina particles allow for easy formation of microcracks which lead to void growth and final failure of the material. Similar structures were observed on the fracture surface of specimens tested at 525K. Again there was strong evidence of bonding between the particles and the matrix alloys.

#### D. Friction and Wear Behavior

The wear tests were carried out on the apparatus shown in Figures 13 and 14. The procedure was that previously described. Photographs of discs removed and machined for use in the wear test machine are shown in Figure 23. The wear tracks made by the 52100 ball bearing can be noted on three of the discs. The uniform distribution of the non-metals is readily noted in the disc containing the coarser  $Al_2O_3$  particles, Figures 23(c) and 23(d). All the tests were done at a constant sliding velocity of 10 cm/sec. The weight loss in each specimen was determined after a given sliding distance. The wear mechanisms were established by examination of both the pin and the wear track using the optical and the scanning electron microscopes.

##### (1) Measured Weight Loss

Measured weight loss (and volume loss) versus sliding distance for a number of the composites determined under different applied loads are shown in Figures 24 to 26. In order to establish the effect of non-metallic additions on the wear behavior each figure contains the average weight loss versus sliding distance data of the matrix alloys liquid forged under identical conditions.



In general, the data in Figures 24 to 26 show that for any given specimen the weight or volume loss continuously increases with increasing sliding distance. Figure 24 displays the wear of 2024 aluminum alloy -  $Al_2O_3$  particle composites under an applied normal load of 50 grams.

The trends established in this figure are; first, the introduction of the hard non-metallic particles reduces the weight loss at a given sliding distance. Second, the weight loss at a given sliding distance decreases with increasing weight percent and size of the  $Al_2O_3$  particles.

Figure 25 shows wear data obtained under different applied load conditions. The two composites contain different weight percentages of  $16\mu m$  size SiC particles. In each composite weight loss increases with increasing applied load. For example, in the composite containing 5 wt% of SiC particles a four fold increase in applied load, from 50 to 200 grams, results in a weight loss which is higher than the matrix alloy. Again, as in Figure 24, increasing the amount of the non-metallic addition results in reduced wear when all other variables are kept constant.

Attempts were made to compare the wear behavior of aluminum alloys containing  $Al_2O_3$  particles and SiC particles, Figure 26. As previously noted, the 2014 and 2024 matrix alloys showed almost similar wear behavior under identical test conditions. Therefore,

it is postulated that the differences in wear behavior noted in Figure 26 can be ascribed to the non-metallic additions. The data show that the SiC particles (Vickers Hardness of 2600) are more effective than the  $Al_2O_3$  particles (Vickers Hardness of 1800) in resisting wear.

Figures 27 and 28 show the measured coefficients of sliding friction as a function of composite composition and applied load. The data show that in general, addition of the non-metallic particles reduced the coefficients of friction. Beyond that, no clear trends relating composition or test conditions to the coefficient of sliding friction could be established.

## (2) Wear Mechanisms

A general observation made in this portion of the investigation was that with increasing additions of non-metals to the aluminum matrices the wear mechanism changed from a purely adhesive to mixed mode of oxidative-abrasive wear. The latter resulted in a corresponding wear of the steel ball bearing. Figure 29 through 31 show the microstructures of a pure matrix alloy, various composition composites and the corresponding ball bearing pins. Figure 29(a) shows the adhesive wear of the aluminum alloy 2014. Metal transfer to the pin in this experiment is shown in Figure 30(a). Addition of 5 wt% of 16 $\mu$ m size  $Al_2O_3$  particles appears to reduce both the plastic flow in the matrix and the metal transfer to the pin, Figures 29(b) and 30(b). When 20 wt% of  $Al_2O_3$  and SiC particles are added to aluminum matrices a dramatic change in the wear mechanism is noted, Figures 29(c), 29(d), 30(c) and 30(d). First, the pin again appears to be riding on the particles and

second, there is evidence of an iron oxide layer on the worn surface of the composites while the pin itself has suffered a purely abrasive wear. Figure 31 shows the microstructures of the aluminum alloy and the composites after further wear, 1000 cycles. Again the adhesive wear mode with extensive plastic flow is noted in the 2014 pure matrix alloy and the low weight percent composite, Figure 31(a) and 31(b). On the other hand, extensive oxidation and some covering of the  $Al_2O_3$  and SiC particles are noted in Figures 31(c) and 31(d).

The flow of the matrix over the non-metallic particles is better illustrated in Figure 32. This figure shows sequences of the microstructure of the wear track of a high non-metal content (20 wt% of  $142\mu m$   $Al_2O_3$ ) composite. The applied load in this experiment was 200 grams. The microstructures reveal that initially the steel ball bearing was essentially riding on the  $Al_2O_3$  particles. Subsequently, beginning with approximately 25 revolutions, either the particles were pushed into the matrix and/or the matrix covered the particles due to plastic flow in the direction of sliding. A second observation made is that while some of the particles appear to have fractured either during the composite fabrication and shape forming or during the wear test there appears to be no particle pullout from the matrix after 2000 revolutions.

Increasing the applied load from 200 to 1000 grams on the 20 wt% non-metal containing composites appeared to change the wear mechanism to a surely abrasive one on both the disc and the pin. While some fine debris are noted, especially on the pin, oxidation of the disk is significantly less than that observed at lower loads,

Figure 33. Correspondingly significant wear of the pin areas noted, Figures 33(c) and 33(d). Lower magnification views of the pins in Figures 33(c) and 33(d) are shown in Figure 34 (a) and 34(b), respectively. These views give an overall picture of the size of the wear track on the pins with respect to the diameter of the ball bearings which was  $\sim 6.4\text{mm}$ .

## V. CONCLUSIONS

1. A technique for the fabrication of aluminum matrix alloy composites containing particulate additions of  $Al_2O_3$  and SiC particles in the size range of 1 to  $142\mu m$  was successfully investigated. The technique uses the special rheological behavior of partially solid, vigorously agitated alloy slurries to entrap the particulate additions until interface interactions promote wetting.
2. Homogeneous additions of the particles in shaped components produced in a forging apparatus were readily obtained except for the very small,  $1\mu m$  in size, particles which clustered during the compositing step.
3. Methods were investigated to both increase the non-metallic content of the composites for improved wear resistance as well as to obtain an abrupt gradient in the composite composition.
4. Low volume fraction composites with the finer,  $5\mu m$  in size, additions of  $Al_2O_3$  show tensile strengths comparable to the matrix alloys. However, in general, the ductility of the composites decreases with increasing volume fraction of non-metallic additions.
5. Aluminum matrices containing high weight percent of hard non-metals exhibit excellent friction and wear properties when tested against a AISI 52100 ball bearing on a pin-on-disk machine. For example, composites of 2024 plus 20 wt% of  $142\mu m$  size  $Al_2O_3$  particles showed a weight loss of  $\sim 2$  orders of magnitude less than the matrix alloy prepared and tested under identical conditions.

6. Aluminum alloys containing SiC particles showed slightly superior wear resistance due to the higher hardness of SiC.

7. Wear mechanism of the matrix alloys under the test conditions was consistently adhesive in nature. On the other hand, composites with high weight percentage of non-metals showed an abrasive wear mechanism on both the disk and the steel ball bearing.

## VI. REFERENCES

1. R. Mehrabian, S. D. E. Ramati, G. J. Abbaschian and D. G. Backman, "Structure and Deformation Characteristics of Rheocast Metals, "Interim Report, December 1977, Contract. No. DAAG46-76-C-0046, AMMRC CTR-77-30, 24 June 1976 to 23 June 1977, prepared for Army Materials and Mechanics Research Center, Watertown, Mass.
2. R. Mehrabian, J. A. Sekhar, C. Y. Chen, G. J. Abbaschian, D. G. Backman, A. Munitz, R. Wunderlin, "Structure and Deformation Characteristics of Rheocast Metals, "Interim Report, January 1979, Contract No. DAAG46-76-C-0046, AMMRC TR-79-2, 24 June 1977 to 23 June 1978, prepared for Army Materials and Mechanics Research Center, Watertown, Mass.
3. W. F. Schilling and N. J. Grant, "Oxide Dispersed Copper Alloys by Surface Oxidation", Met. Trans. V. 1, Aug. 1970, p. 2205-2210.
4. O. Preston and N. J. Grant, "Dispersion Strengthening of Copper by Internal Oxidation", Trans. Met. Soc. AIME, V. 221, 1961, p. 164-173.
5. W. S. Cremens and N. J. Grant, "Preparation and High Temperature Properties of Nickel- $Al_2O_3$  Alloys", Proc. ASTM, V. 58, 1958, p. 714-732.
6. R. Mehrabian, R. G. Riek and M. C. Flemings, "Preparation and Casting of Metal-Particulate Non-Metal Composites", Met. Trans., V. 5, 1974, p. 1899-1905.
7. A. Sato and R. Mehrabian, "Aluminum Matrix Composites: Fabrication and Properties", Met. Trans. V. 7B, 1976, p. 443-451.
8. B. I. Edelson and W. M. Baldwin Jr., "The Effect of Second Phases on the Mechanical Properties of Alloys", Trans. ASM, V. 55, 1962, p. 230-251.
9. I. L. Mogford, "The Deformation and Fracture of Two-Phase Materials", Met. Reviews, V. 12, 1967, p. 49-68.
10. C. G. Levi, G. J. Abbaschian and R. Mehrabian, "Interface Interactions During Fabrication of Aluminum Alloy - Alumina Fiber Composites", Met. Trans., V. 9A, May, 1978, p. 697-711.
11. H. Czichos, Tribology, Amsterdam: Elsevier Scientific Publishing Co., 1978, pp. 84-121.

12. M. M. Khrushov, "Principles of Abrasive Wear", Wear, Vol. 28, 1974, p. 69.
13. D. A. Rigney and W. A. Glaeser, Source Book on Wear Control Technology, ASM, Metals Park, OH, pp. 1-10.
14. N. P. Suh, "The Delamination Theory of Wear", Wear, Vol. 25, 1973, p. 111.
15. J. F. Archard, "Contact and Rubbing of Flat Surfaces", J. App. Phys., Vol. 24, 1953, p. 981.
16. K. J. Bhansali, "Adhesive Wear of Nickel and Cobalt-base Alloys". Paper presented at the International Conference on Wear of Materials, The American Society of Mechanical Engineers, April 1979.
17. S. Hogmark, O. Vinth and S. Fridstrom, "Mechanisms of Dry Wear of Some Martensitic Steels", Wear, Vol. 31, 1975, pp. 39-61.
18. T. F. Quinn, J. L. Sullivan and D. M. Rowson, "New Developments in the Oxidational Theory of the Mild Wear of Metals". Paper presented at the International Conference on Wear of Materials, The American Society of Mechanical Engineers, April 1979.
19. V. Gologan and T. S. Eyre, "Friction and Wear of Some Engineering Materials Against Hard Chromium Plating", Wear, Vol. 28, 1974, pp. 49-57.
20. R. D. Arnell, A. P. Herod and D. G. Teer, "The Effect of Combined Stresses on the Transition from Mild to Severe Wear", Wear, Vol. 31, 1975, pp. 237-242.
21. A. V. Lineal and H. E. Hintermann, "Boronizing Processes - A Tool for Decreasing Wear". Paper presented at the International Conference on Wear of Materials, The American Society of Mechanical Engineers, April 1979.
22. A. Sato and R. Mehrabian, "Aluminum Matrix Composites: Fabrication and Properties", Met. Trans., Vol. 7B, 1976, p. 443.
23. D. Nath, S. K. Biswas and P. K. Rohatgi, "Wear Characteristics and Bearing Performance of Aluminum-Mica Particulate Composite Material". Paper presented at the International Conference on Wear of Materials, The American Society of Mechanical Engineers, April 1979.
24. C. Beesley and T. S. Eyre, "Friction and Wear of Aluminum Alloys Containing Copper and Zinc", Tribology Int., Vol. 9, No. 2, 1976, pp. 63-69.



25. R. Shivanath, P. K. Sengupta and T. S. Eyre, "Wear of Aluminum-Silicon Alloys", Source Book on Wear Control Technology, American Society of Metals, Metals Park, OH, 1978.
26. A. D. Sarkar, "Wear of Aluminum-Silicon Alloys", *Wear* Vol. 31, 1975, pp. 331-343.
27. C. G. Levi, G. J. Abbaschian and R. Mehrabian, "Interface Interactions During Fabrication of Aluminum Alloy - Alumina Fiber Composites", *Met. Trans.*, Vol. 9A, May 1978, p. 697-711.
28. J. T. Burwell and C. D. Strange, "On the Empirical Law of Adhesive Wear", *J. Appl. Physics*, Vol. 23, No. 1, 1953, p. 18.
29. L. C-Y. Wu, "The Adhesion, Friction and Wear of Sputtered Titanium Carbide Coatings on Polished Steel Substrates", M. S. Thesis, Department of Mechanical Engineering, University of Illinois at Urbana-Champaign, 1976.
30. *Metals Handbook*, V. 1, ASM.
31. F. R. Mollard, "K0-1 Aluminum Casting Alloy - X1 - Influence of Iron and Silicon Impurities on Room Temperature Tensile Properties", unpublished report, Conalco, Inc.
32. A. Munitz, M. Metzger and R. Mehrabian, "The Interface Phase in Al-Mg/Al<sub>2</sub>O<sub>3</sub> Composites", *Met. Trans. A*, V. 10A, p. 1491, (1979).

TABLE I

Classification of the types of wear by Czichos (11)

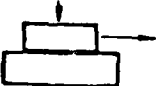

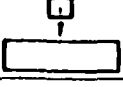



Interacting elements	<div>Wear mechanisms</div> <div>Type of relative motion</div>	mainly stress interactions		stress + material interactions	
		surface fatigue	abrasion	adhesion	tribo-chemical
solid/solid (metals, polymers, minerals, etc.) without or with lubricants	 sliding	sliding wear			
	 rolling	rolling wear			
	 impact	impact wear			
	 oscillation	fretting wear			
solid/liquid	 flow	cavitation wear			
solid/fluid + particles	 flow	fluid erosion			

TABLE II

Sample Identification and Composition of the Composites Fabricated and Tested

<u>Specimen Identification</u>	<u>Matrix Alloy</u>	<u>Particles charged*</u>	
		<u>Size (<math>\mu\text{m}</math>)</u>	<u>Weight % charged</u>
2024	2024	-	-
2024-10% ( $1\mu\text{m Al}_2\text{O}_3$ )	2024	1	10.0**
2024-2% ( $5\mu\text{m Al}_2\text{O}_3$ )	2024	5	2.0**
2024-5% ( $5\mu\text{m Al}_2\text{O}_3$ )	2024	5	5.0**
2024-20% ( $5\mu\text{m Al}_2\text{O}_3$ )	2024	5	20.0**
2024-5% ( $16\mu\text{m Al}_2\text{O}_3$ )	2024	16	5.0**
2024-20% ( $16\mu\text{m Al}_2\text{O}_3$ )	2024	16	20.0**
2024-20% ( $63\mu\text{m Al}_2\text{O}_3$ )	2024	63	20.0**
2024-20% ( $142\mu\text{m Al}_2\text{O}_3$ )	2024	142	20.0**
2024-30% ( $142\mu\text{m Al}_2\text{O}_3$ )	2024	142	30.0**
2014	2014	-	-
2014-2% ( $1\mu\text{m Al}_2\text{O}_3$ )	2014	1	2.0**
2014-5% ( $1\mu\text{m Al}_2\text{O}_3$ )	2014	1	5.0**
2014-2% ( $5\mu\text{m Al}_2\text{O}_3$ )	2014	5	2.0**
2014-5% ( $5\mu\text{m Al}_2\text{O}_3$ )	2014	5	5.0**
2014-5% ( $16\mu\text{m Al}_2\text{O}_3$ )	2014	16	5.0**
2014-5% ( $63\mu\text{m Al}_2\text{O}_3$ )	2014	63	5.0**
2014-20% ( $16\mu\text{m Al}_2\text{O}_3$ )	2014	16	20.0**
2014-5% ( $16\mu\text{m SiC}$ )	2014	16	5.0**
2014-20% ( $16\mu\text{m SiC}$ )	2014	16	20.0**
201	201	-	-
201-5% ( $5\mu\text{m Al}_2\text{O}_3$ )	201	5	5.0**

\*  $\text{Al}_2\text{O}_3$ : Unfused Alpha Alumina (Platey, Sharp Morphology)

\*\* : Specimens subjected to wear tests.

TABLE III

HEAT TREATMENT OF LIQUID FORGED SPECIMENS

<u>ALUMINUM ALLOY MATRIX</u>	<u>CONDITION</u>	<u>TEMPERATURE (K)</u>	<u>TIME (HR.)</u>	<u>QUENCH</u>
2014 <sup>*</sup>	Solutionize	769	24.0	Cold Water
2014 <sup>*</sup>	T4	R.T. <sup>†</sup>	48.0	—
2014 <sup>*</sup>	T6	444	10.0	Air
2024 <sup>*</sup>	Solutionize	769	24.0	Cold Water
2024 <sup>*</sup>	T4	R.T. <sup>†</sup>	48.0	—
2024 <sup>*</sup>	T6	459	12.0	Air
201 <sup>**</sup>	Solutionize	808	24.0	Cold Water
201 <sup>**</sup>	T4	R.T. <sup>†</sup>	120.0	—
201 <sup>**</sup>	T6	427	15.0	Air

<sup>†</sup>R.T. - Room Temperature

<sup>\*</sup>Heat Treatment from reference [30]

<sup>\*\*</sup>Heat Treatment from reference [31]

TABLE IV

Tensile Properties of Heat Treated Commercial  
Aluminum Alloys

<u>Material</u>	<u>Ultimate Tensile Strength, Kg/mm<sup>2</sup></u>	<u>0.2% Offset Yield Strength Kg/mm<sup>2</sup></u>	<u>% Elongation</u>
2014-T4 <sup>a</sup>	41.2	22.6	25.0
2014-T6 <sup>b</sup>	43.6	38.1	12.6
2024-T6 <sup>c</sup>	48.3	36.2	13.4
2024-T6 <sup>d</sup>	46.4	34.7	11.2
2024-T4 [Ref. 30]	45.7	33.1	20.0
2024-T6 [Ref. 30]	48.5	40.0	10.0
KO-1-T4 [Ref. 31]	35.2	21.1	12.0
KO-1-T6 [Ref. 31]	37.3	32.4	4.0

a - Specimens pulled from as-received wrought stock treated to T4 condition.

b - Specimens pulled from as-received wrought stock in T-651 condition.

c - Squeeze cast (liquid forged) specimens produced in an earlier study [ 2 ].

d - Thixoforged (forged when the alloy was in partially solid, Rheocast state) specimens produced in an earlier study [ 2 ].

TABLE V

Room Temperature Mechanical Properties of Liquid Forged Composites and Matrix Alloys  
Heat Treated to T4 - Condition

Specimen	Ultimate Tensile Strength, Kg/mm <sup>2</sup>	0.2% Offset Yield Strength Kg/mm <sup>2</sup>	% Elongation	% Reduction Area	Ductility (ln A <sub>0</sub> /A <sub>f</sub> )
2024	38.8	26.8	8.2	6.3	0.065
2024-10% (1μm Al <sub>2</sub> O <sub>3</sub> )	21.3	-	0.6	1.6	0.016
2024-2% (5μm Al <sub>2</sub> O <sub>3</sub> )	31.9	24.0	2.8	4.0	0.041
2024-5% (5μm Al <sub>2</sub> O <sub>3</sub> )	34.5	24.9	3.4	4.8	0.050
2024-20% (5μm Al <sub>2</sub> O <sub>3</sub> )	16.5	-	0.5	0.8	0.008
2024-5% (16μm Al <sub>2</sub> O <sub>3</sub> )	32.5	25.9	2.2	4.0	0.041
2024-20% (16μm Al <sub>2</sub> O <sub>3</sub> )	13.9	-	0.4	0.0	0.000
2024-20% (142μm Al <sub>2</sub> O <sub>3</sub> )	20.7	-	0.3	0.0	0.000
2024-30% (142μm Al <sub>2</sub> O <sub>3</sub> )	15.4	-	0.2	0.0	0.000
2014	32.0	21.3	7.0	7.1	0.073
2014-2% (1μm Al <sub>2</sub> O <sub>3</sub> )	25.4	20.2	1.6	3.9	0.033
2014-5% (1μm Al <sub>2</sub> O <sub>3</sub> )	22.4	20.8	1.0	1.6	0.016
2014-2% (5μm Al <sub>2</sub> O <sub>3</sub> )	34.3	23.5	5.7	6.3	0.065
2014-5% (5μm Al <sub>2</sub> O <sub>3</sub> )	31.9	22.0	5.1	7.1	0.073
2014-5% (16μm Al <sub>2</sub> O <sub>3</sub> )	30.9	22.5	4.2	4.0	0.040
2014-5% (63μm Al <sub>2</sub> O <sub>3</sub> )	29.6	21.4	3.4	6.3	0.065
201	34.1	18.9	14.0	21.0	0.237
201-5% (5μm Al <sub>2</sub> O <sub>3</sub> )	27.7	21.6	2.6	3.6	0.040

TABLE VI

Room Temperature Properties of Liquid Forged Matrix Alloy  
(Heat Treated to T6 - condition)

<u>Specimen</u>	<u>Ultimate Tensile Strength, Kg/mm<sup>2</sup></u>	<u>0.2% Offset Yield Strength Kg/mm<sup>2</sup></u>	<u>% Elongation</u>	<u>% Reduction Area</u>
2024	40.7	33.6	3.5	4.0
2014	42.6	36.7	2.6	3.2
201	36.8	32.4	4.4	6.2
2024 <sup>a</sup>	48.3	36.2	13.4	-
2024 <sup>b</sup>	46.4	34.7	11.2	-

a - Squeeze Cast, liquid forged, specimens produced in an earlier study [ 2 ].

b - Thixoforged specimens produced in an earlier study [ 2 ].

TABLE VII

Elevated Temperature (525K) Properties of Liquid Forged  
Composites and Matrix Alloys Heat Treated to a T-4 Condition

<u>Specimen</u>	<u>Ultimate Tensile Strength, Kg/mm<sup>2</sup></u>	<u>% Elongation</u>	<u>% Reduction Area</u>
2024	26.5	10.0	10.9
2024-10% (1 $\mu$ m Al <sub>2</sub> O <sub>3</sub> )	9.0	1.4	2.4
2024-5% (5 $\mu$ m Al <sub>2</sub> O <sub>3</sub> )	24.2	2.0	2.4
2024-5% (16 $\mu$ m Al <sub>2</sub> O <sub>3</sub> )	24.0	2.5	3.2
2014	23.5	9.0	10.2
2014-2% (1 $\mu$ m Al <sub>2</sub> O <sub>3</sub> )	10.0	4.5	4.7
2014-5% (1 $\mu$ m Al <sub>2</sub> O <sub>3</sub> )	20.0	3.0	3.9
2014-2% (5 $\mu$ m Al <sub>2</sub> O <sub>3</sub> )	16.8	7.5	7.1
2014-5% (5 $\mu$ m Al <sub>2</sub> O <sub>3</sub> )	21.0	2.5	4.0
2014-5% (16 $\mu$ m Al <sub>2</sub> O <sub>3</sub> )	18.5	3.0	6.3
2014-5% (63 $\mu$ m Al <sub>2</sub> O <sub>3</sub> )	21.2	5.0	7.0
201	25.2	21.0	19.7
201-5% (5 $\mu$ m Al <sub>2</sub> O <sub>3</sub> )	20.9	6.5	7.0



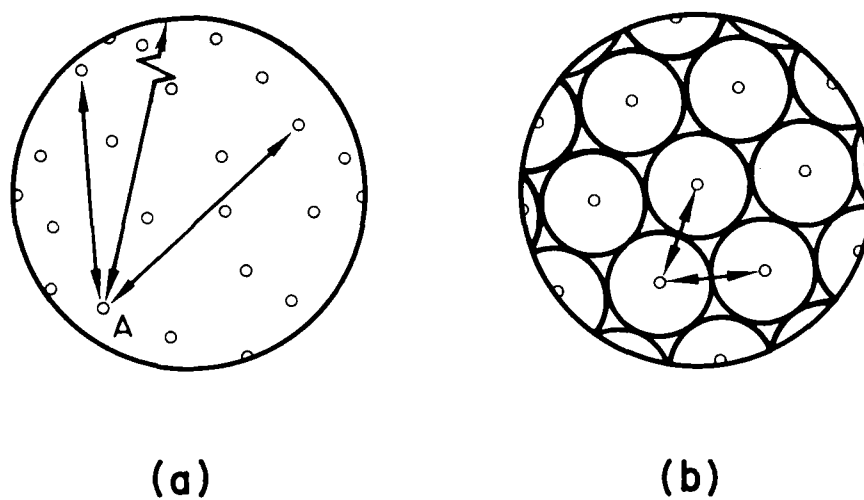


Figure 1. Illustration of two measurements of particle spacing: (a) Mean free path between particles ( $\lambda$ ) and (b) Interparticle Spacing ( $D_s$ ). From reference [8].

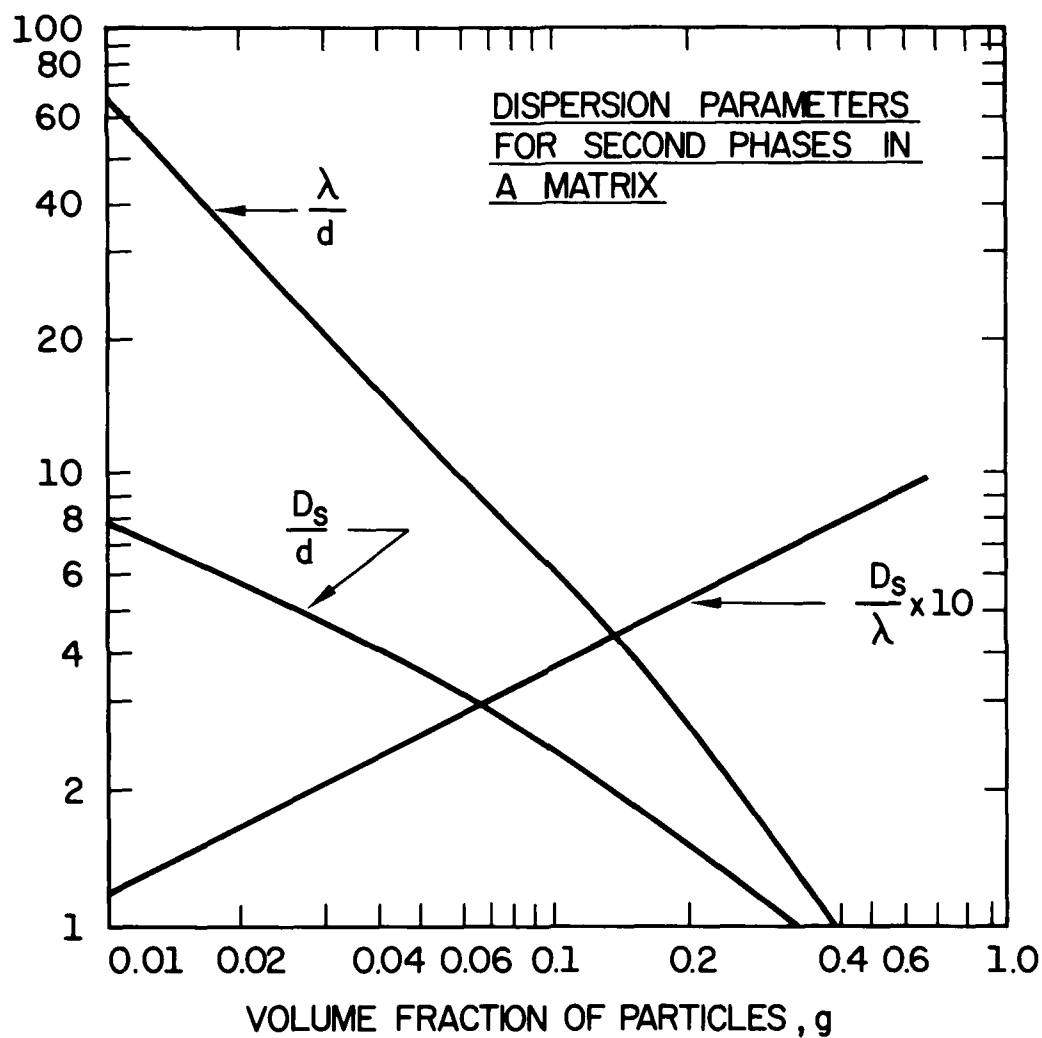


Figure 2. Relationships between volume fraction ( $g$ ), particle diameter ( $d$ ), interparticle spacing ( $D_s$ ) and mean free path ( $\lambda$ ). From equations (1) to (3).

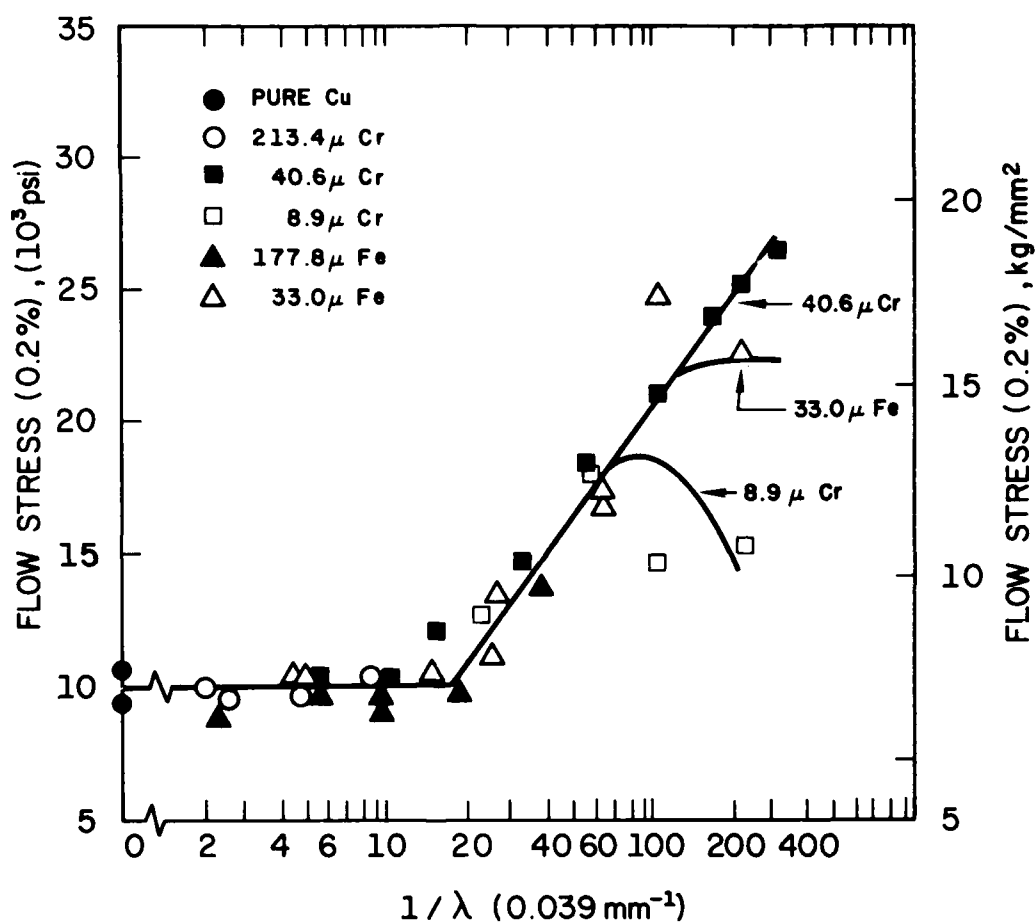


Figure 3. The relation of yield stress to log reciprocal mean free path between particles in copper-chromium and copper-iron alloys (Gensamer plot). From reference [8].

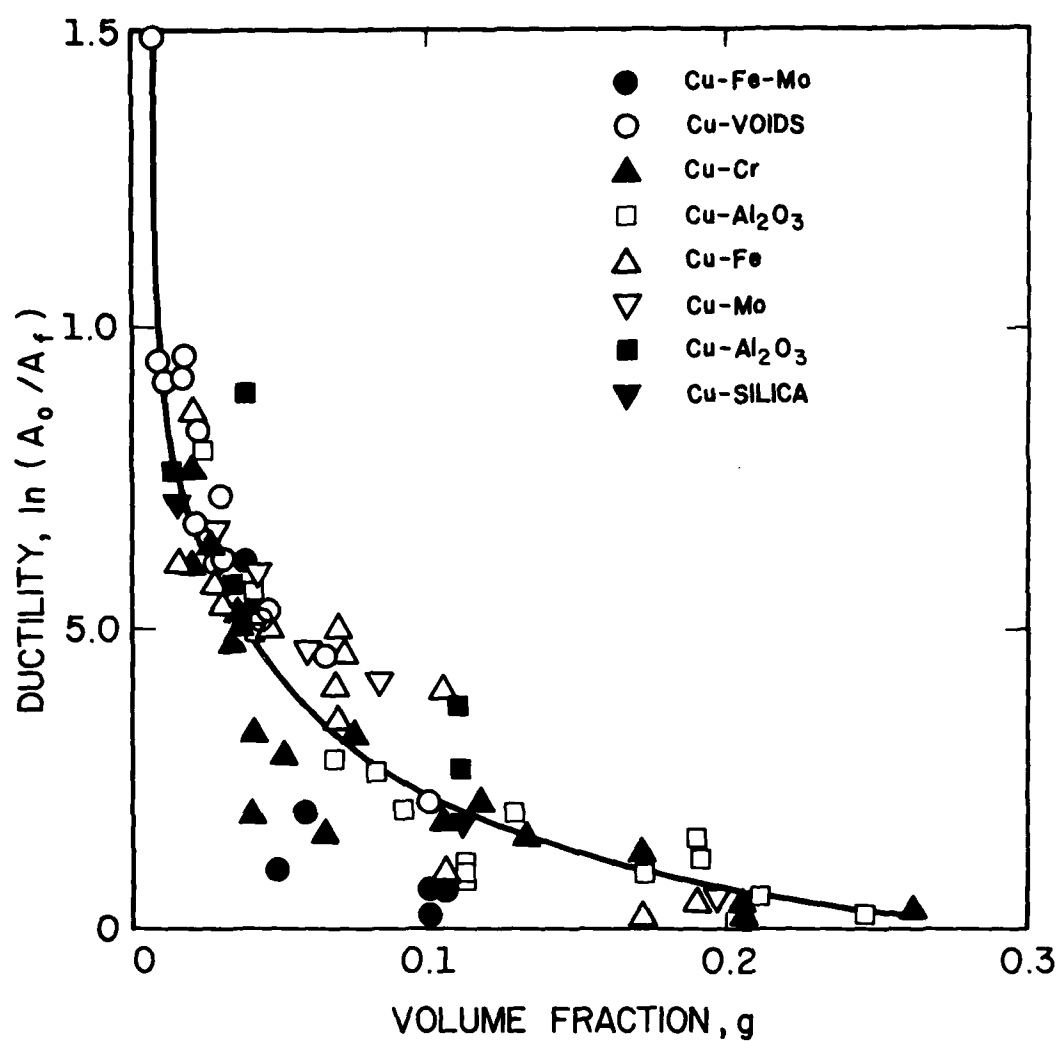


Figure 4. Combined plot of ductility of several copper dispersion alloys versus volume fraction. From reference [8].

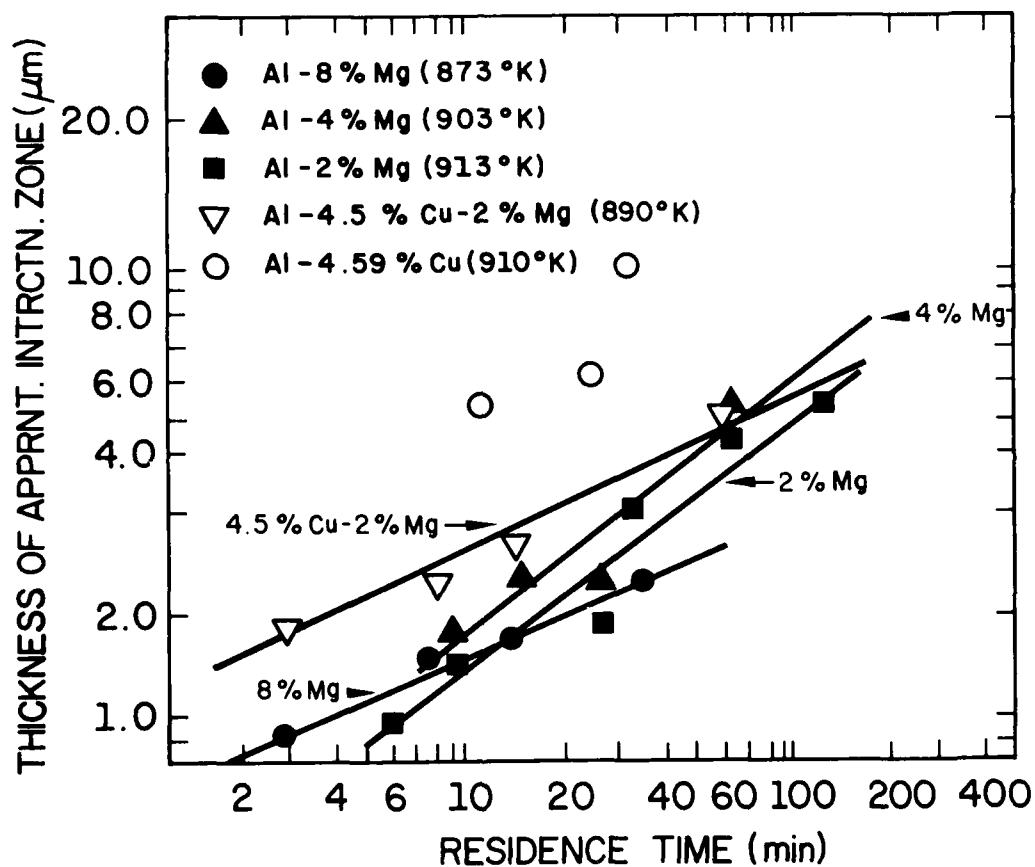
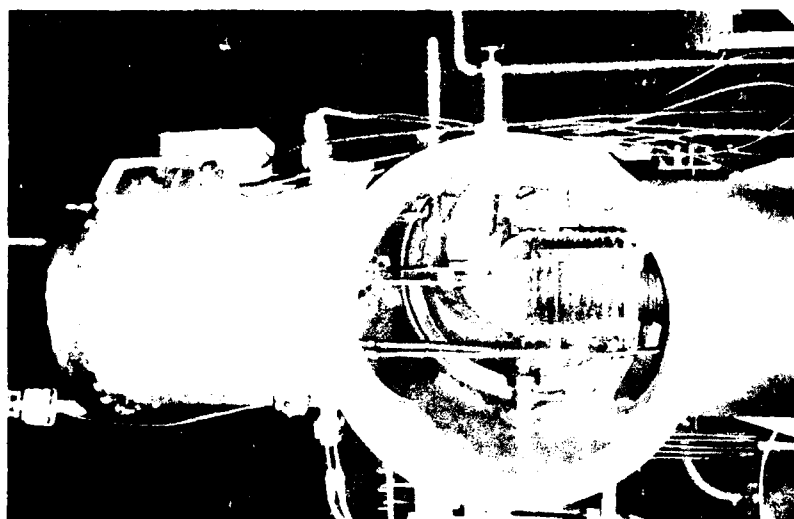
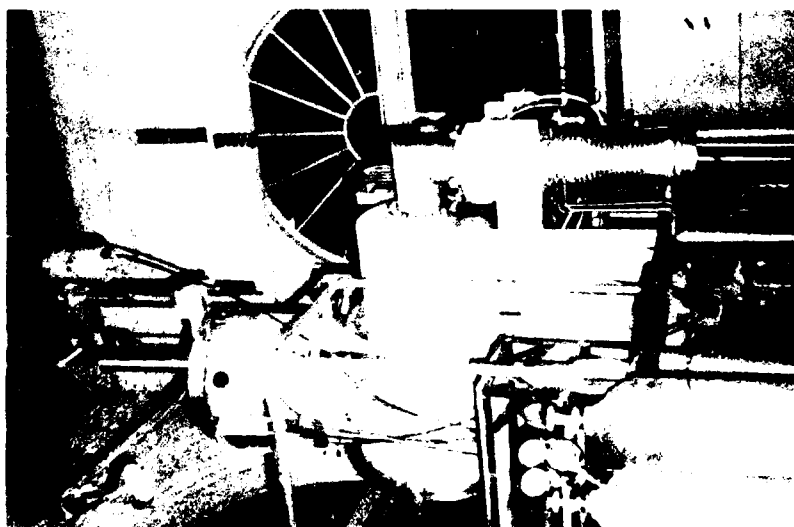


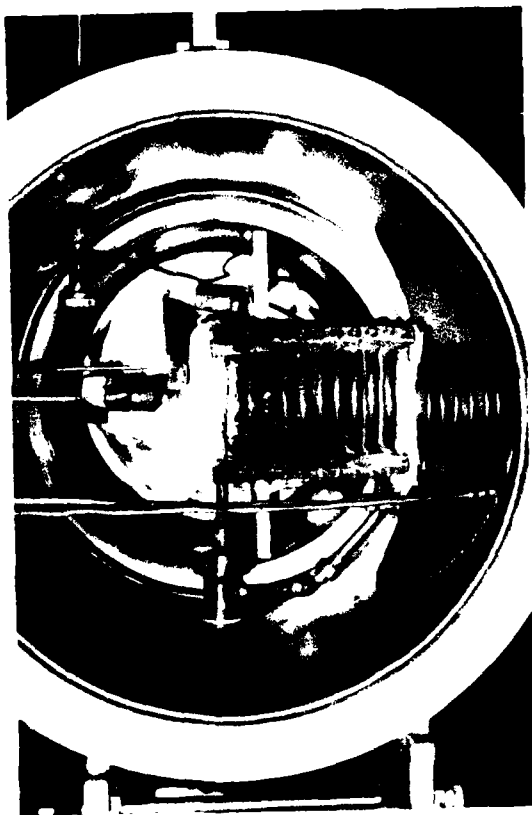
Figure 5. Average maximum thickness of the "apparent interaction zone" as a function of residence time. From reference [10].



(b)



(a)



(c)

Figure 6. Photographs of the compositing apparatus. (a) shows an overall view of the vacuum system on its stand with its associated pumps, mixing motor etc. (b) and (c) show close-ups of the chamber, the induction coil, mixing blade and particle addition trough.

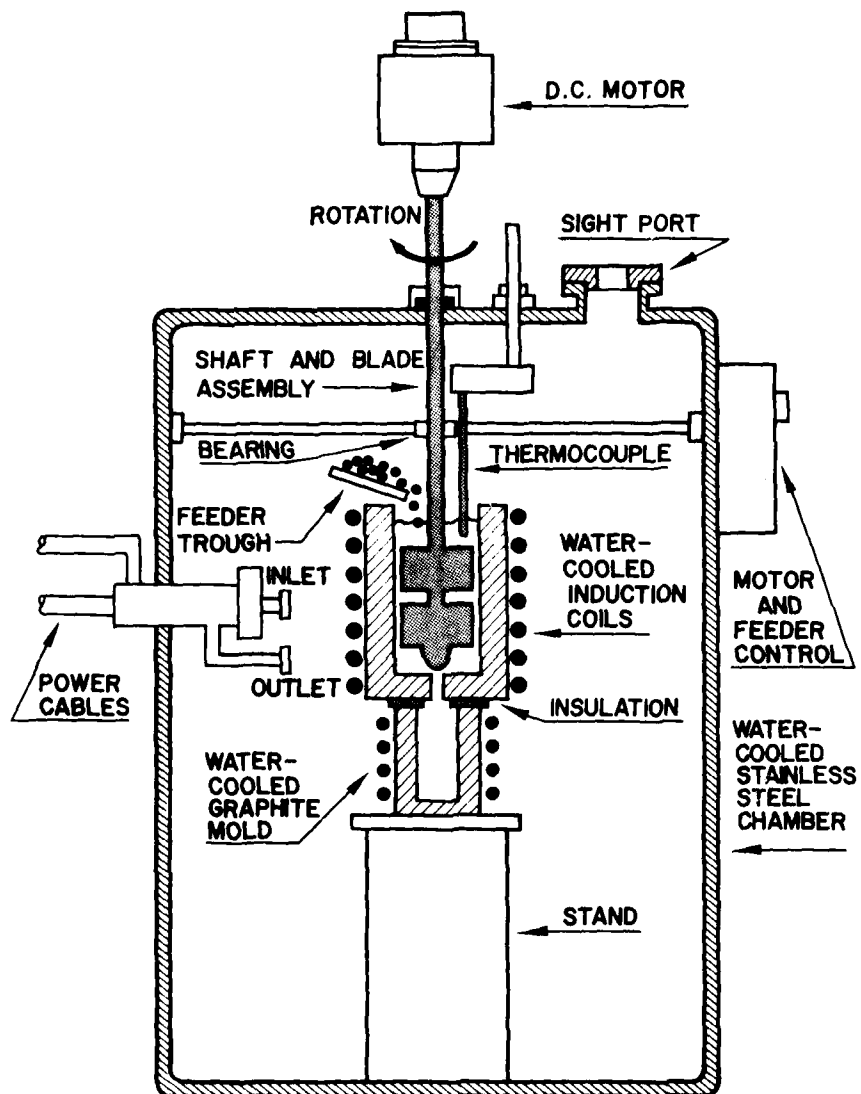
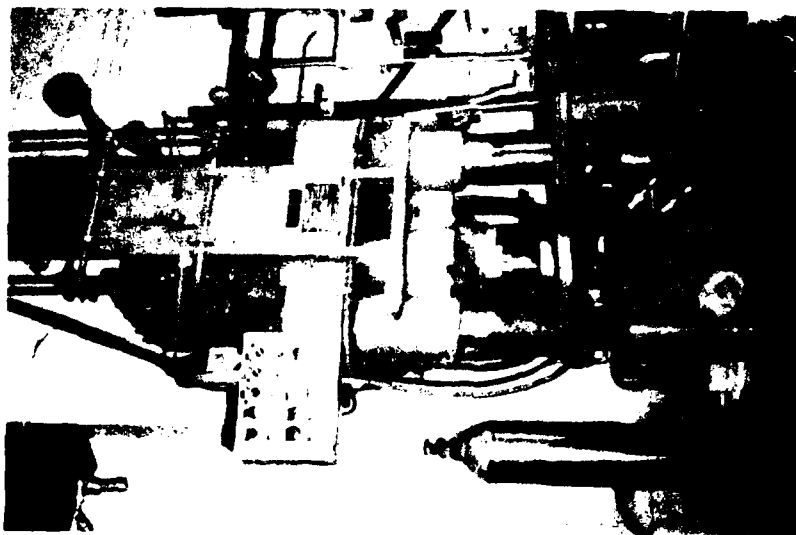


Figure 7. Schematic illustration of the compositing apparatus.





(a)



(b)

Figure 8. Photographs of the liquid forging apparatus. (a) shows the 200-ton hydraulic press and (b) shows the induction reheating system with its associated power supplies.



(a)



(b)

Figure 9. Photographs of the forging die in the hydraulic press and the part produced. (a) shows a disc-shaped part ~ 115mm in diameter by ~ 40mm tall. (b) Shows the steel ring insert used in the lower die half to produce the reduced cross-section disc-shape on the right.

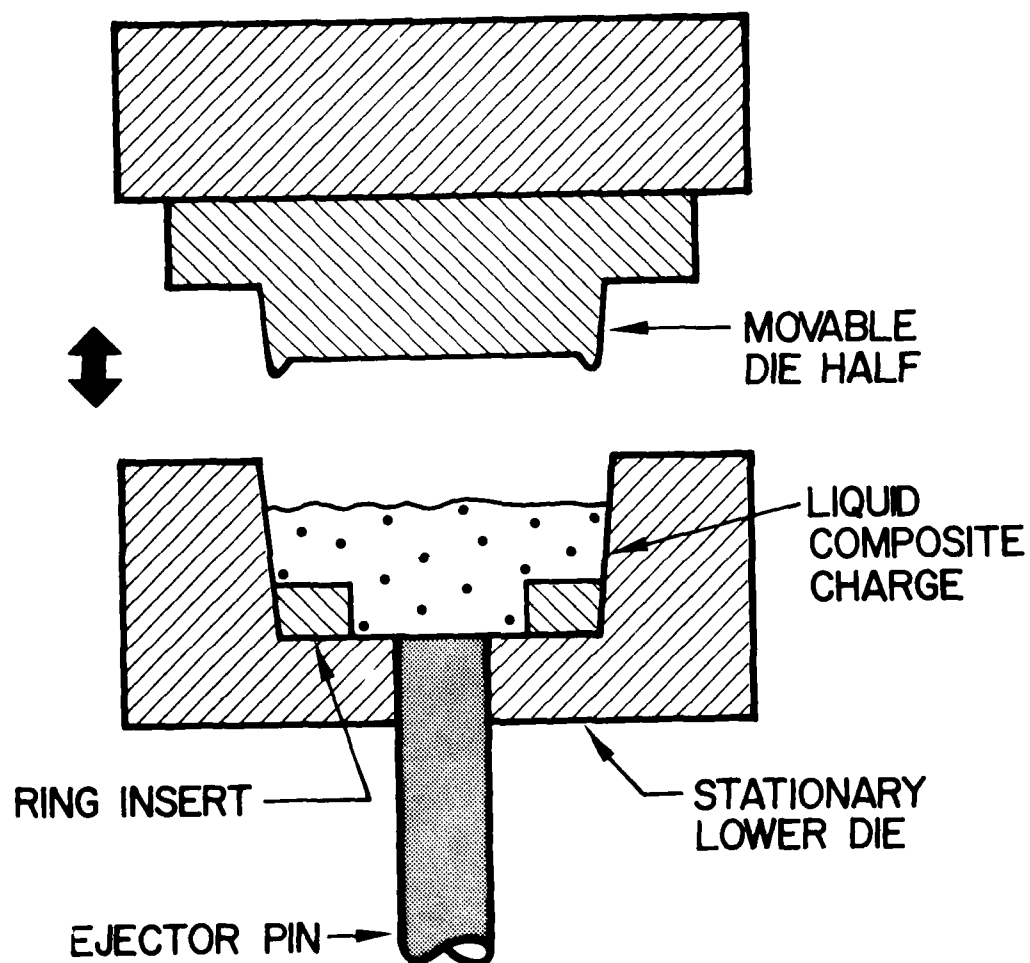


Figure 10. Schematic illustration of the forging dies used in forming of the aluminum matrix composites in the hydraulic press.

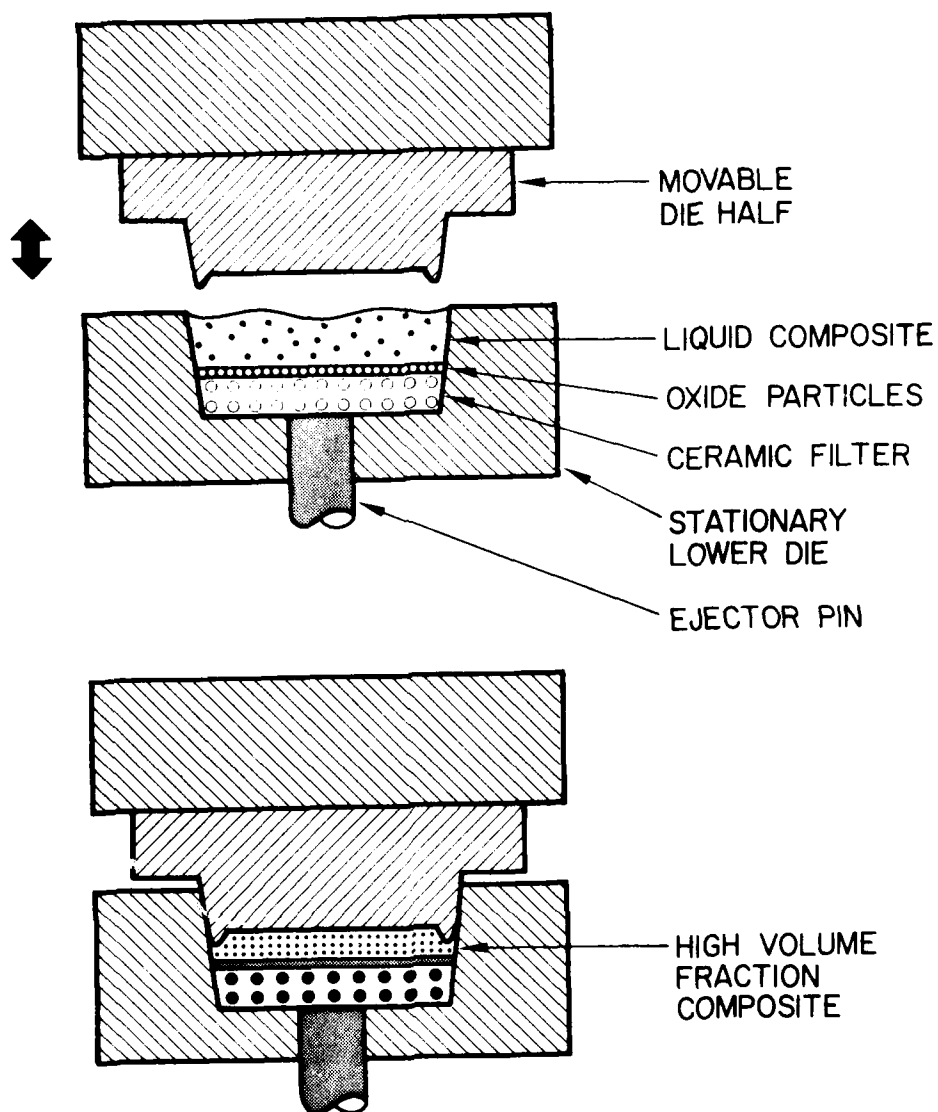
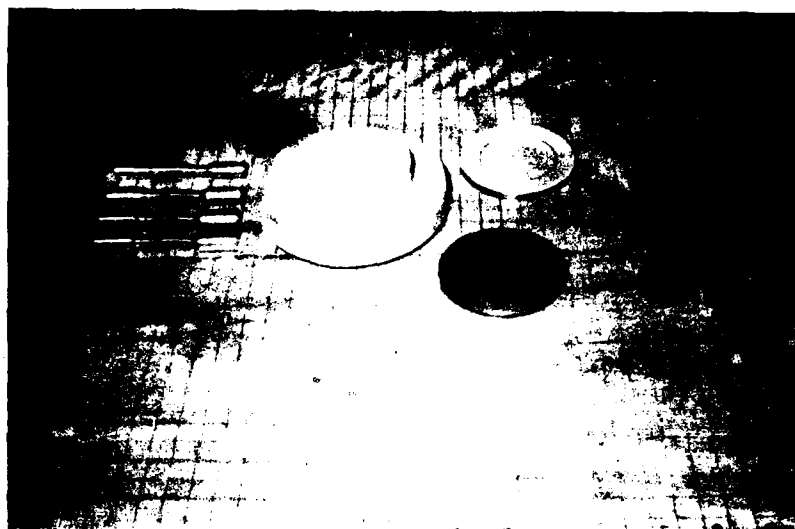


Figure 11. Schematic illustration of the die set-up used to fabricate high volume fraction composites of aluminum alloys.



(a)

Figure 12. Photograph showing an aluminum matrix composite in the as-forged condition with sections removed and machined from a similar part for wear and tensile tests.

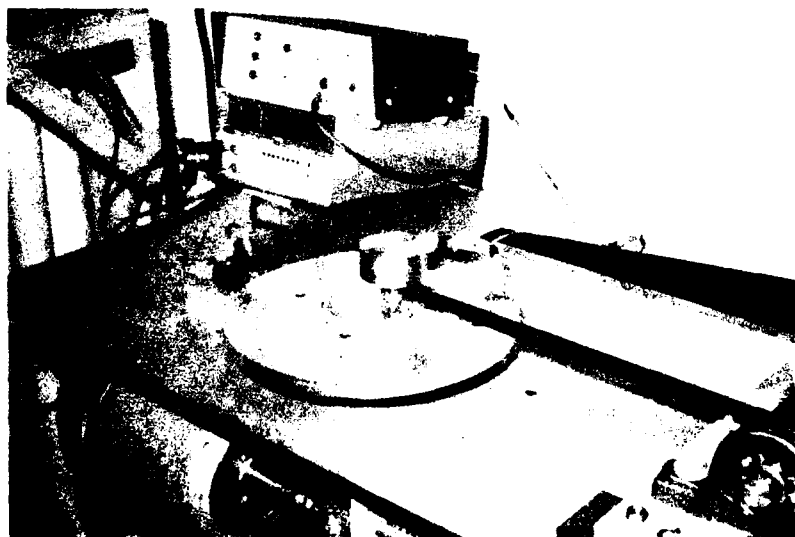
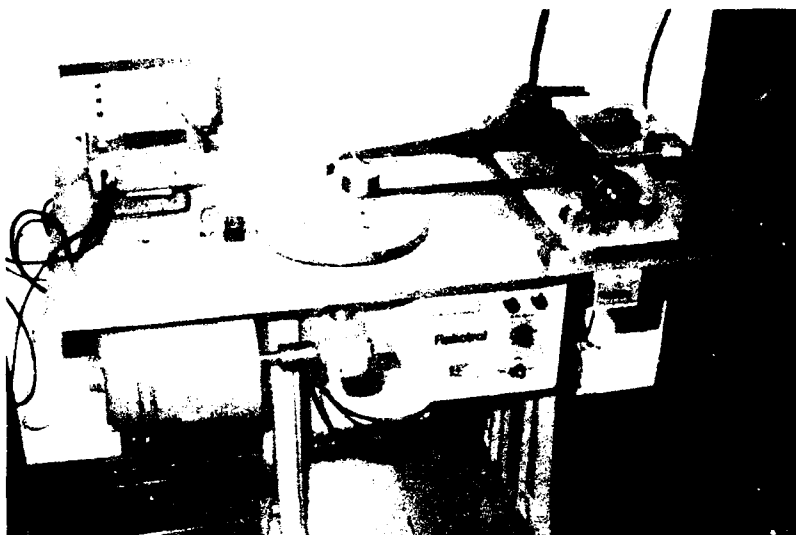


Figure 13. Photographs of the pin-on-disc wear test machine built and used in this investigation.

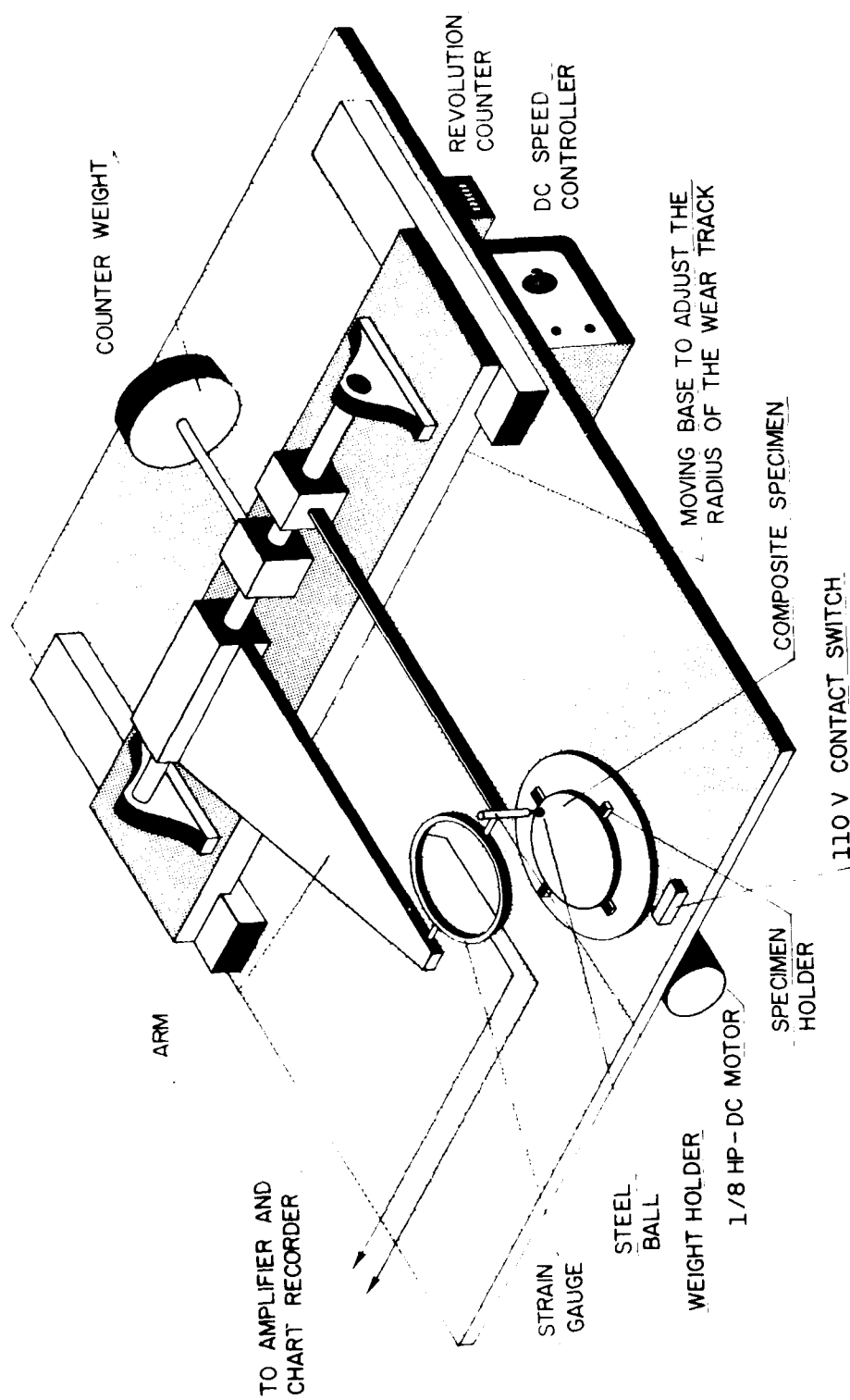


Figure 14. Schematic illustration of the wear test machine.



(a)



(b)

Figure 15. SEM photomicrographs of liquid forged composites of aluminum alloy containing 5 weight percent of  $\text{Al}_2\text{O}_3$  particles. (a)  $\text{Al}_2\text{O}_3$  particles in a 2024 aluminum alloy at 400x magnification. (b)  $\text{Al}_2\text{O}_3$  particles in a 2014 aluminum alloy at 400x magnification.





Figure 16. SEM photomicrographs of liquid forged composites of aluminum alloys containing 20 weight percent of Al<sub>2</sub>O<sub>3</sub> particles at 45X. (a) 16 $\mu$ m particles in a 2014 aluminum alloy, (b) 63 $\mu$ m particles in a 2024 aluminum alloy, (c) 142 $\mu$ m particles in a 2024 aluminum alloy.

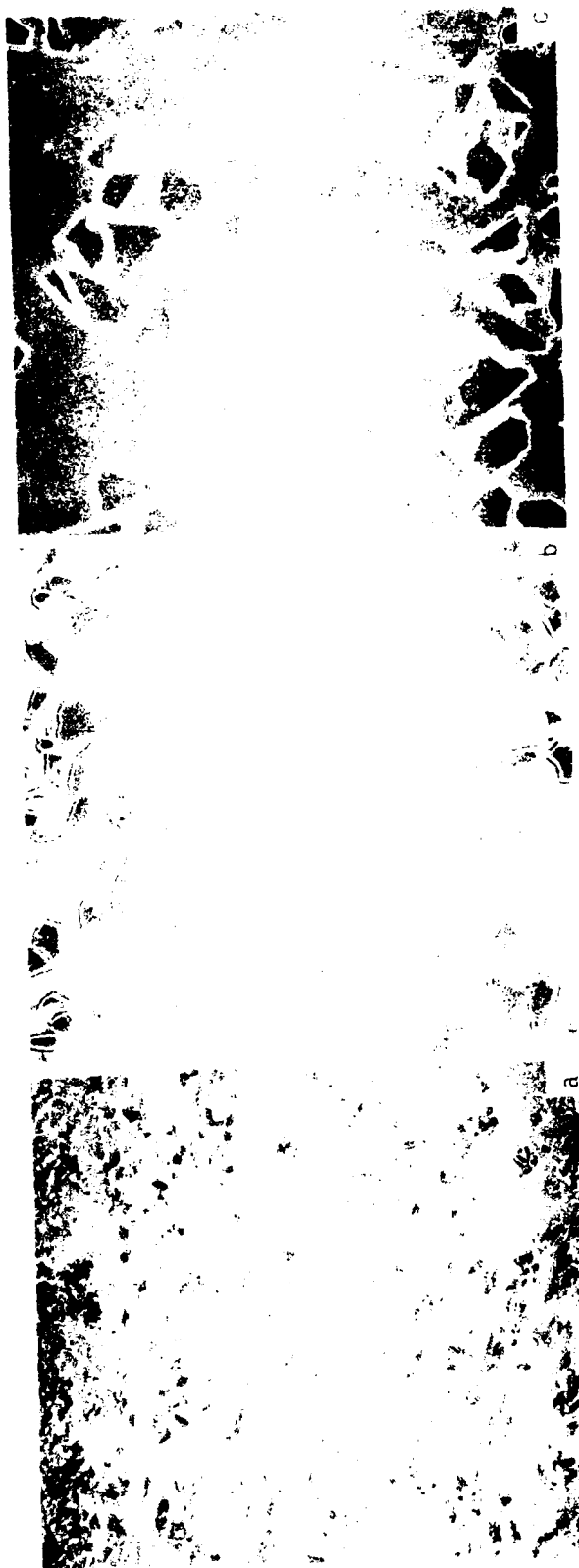
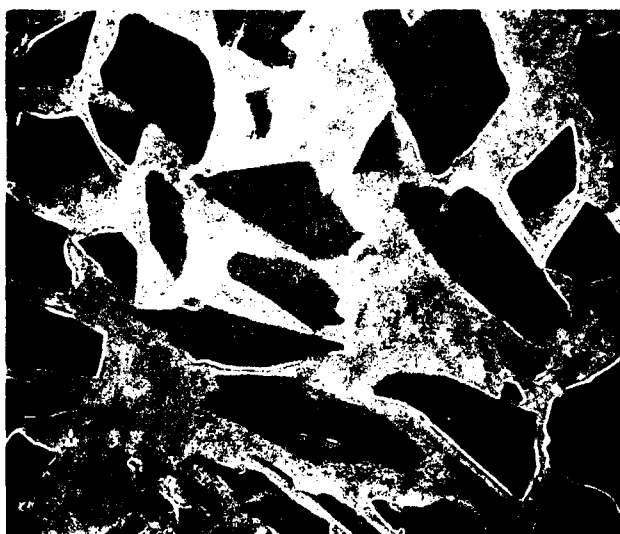


Figure 17. SEM photomicrographs of liquid forged composites of aluminum alloys containing 20 weight percent of  $Al_2O_3$  particles at 100X. (a) 16 $\mu m$  particles in a 2014 aluminum alloy, (b) 63 $\mu m$  particles in a 2024 aluminum alloy, (c) 142 $\mu m$  particles in a 2024 aluminum alloy.



(a)

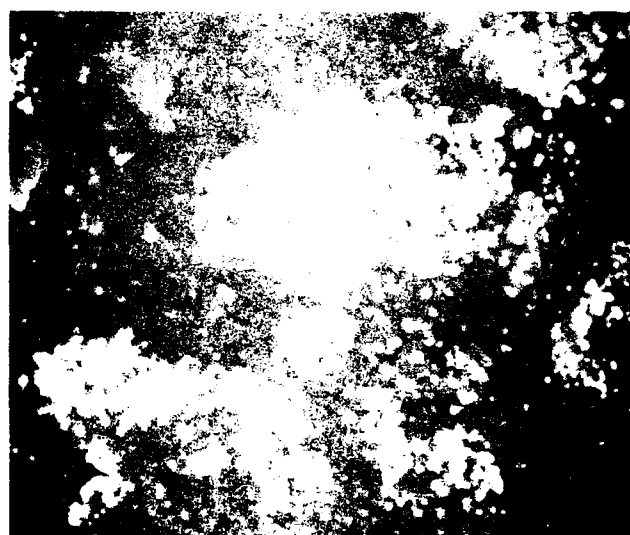


(b)

Figure 18. SEM photomicrographs of a liquid forged composite of 2024 aluminum alloy containing 30 weight percent of 142 $\mu$ m size  $Al_2O_3$  particles. (a) 100X, (b) 200X.

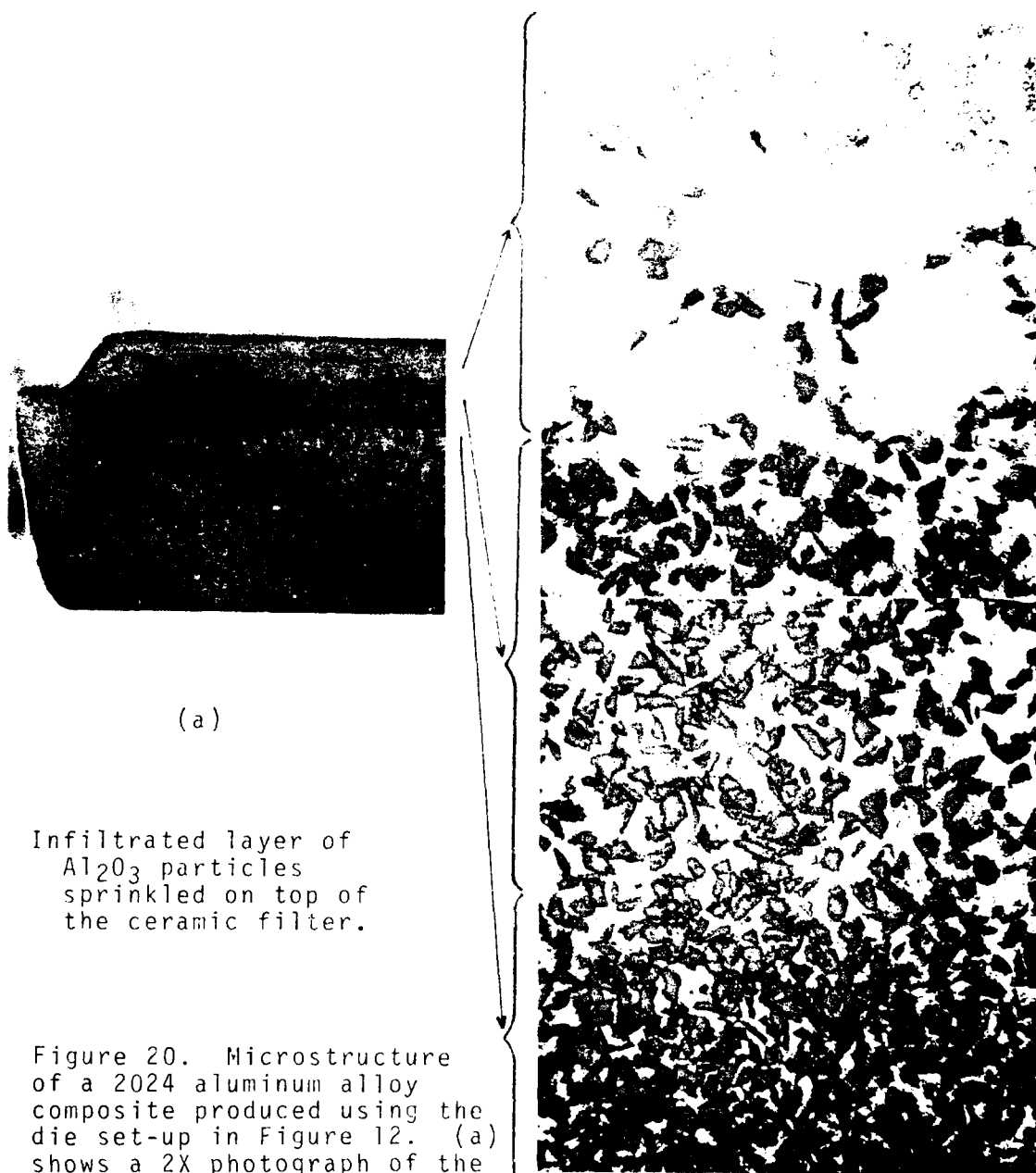


(a)



(b)

Figure 19. SEM photomicrographs of liquid forged composites of aluminum alloy 2014 alloy matrix containing 5 weight percent of 1  $\mu$ m size  $Al_2O_3$  particles at 450X, (b) 2014 alloy matrix containing 5 weight percent of 1  $\mu$ m size  $Al_2O_3$  particles at 3000X.



(a)

Infiltrated layer of  
 $\text{Al}_2\text{O}_3$  particles  
 sprinkled on top of  
 the ceramic filter.

Figure 20. Microstructure of a 2024 aluminum alloy composite produced using the die set-up in Figure 12. (a) shows a 2X photograph of the dual layered composite with a high volume fraction of  $142\mu\text{m}$   $\text{Al}_2\text{O}_3$  particles in its lower half. The upper half is the infiltrated ceramic filter. (b) is a high magnification view of the microstructure above the filter. It consists of a matrix devoid of particles, a high volume fraction of  $142\mu\text{m}$  and infiltrated but not wetted  $\text{Al}_2\text{O}_3$  particles sprinkled on top of the filter to prevent the composite particles from entering the filter.

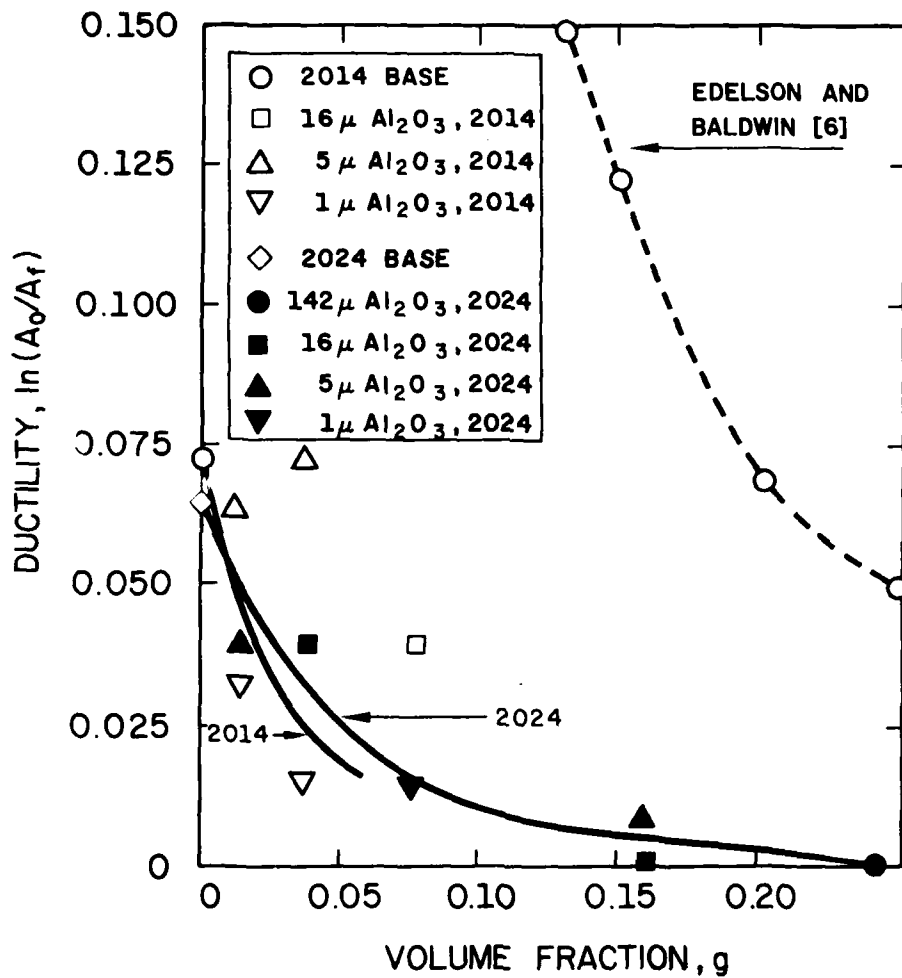
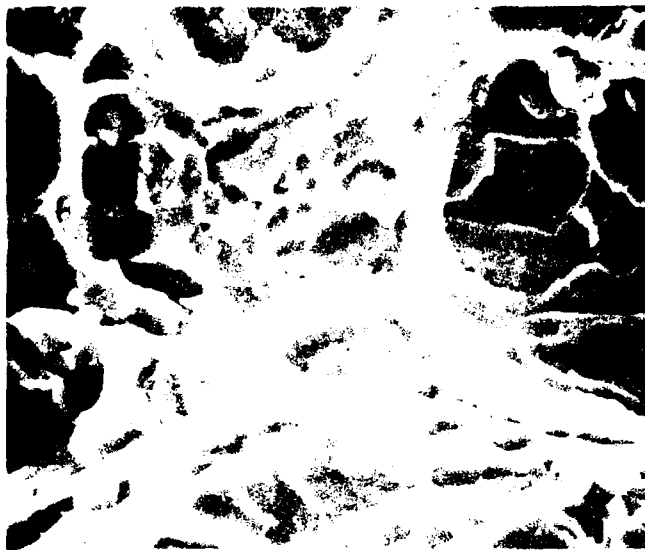
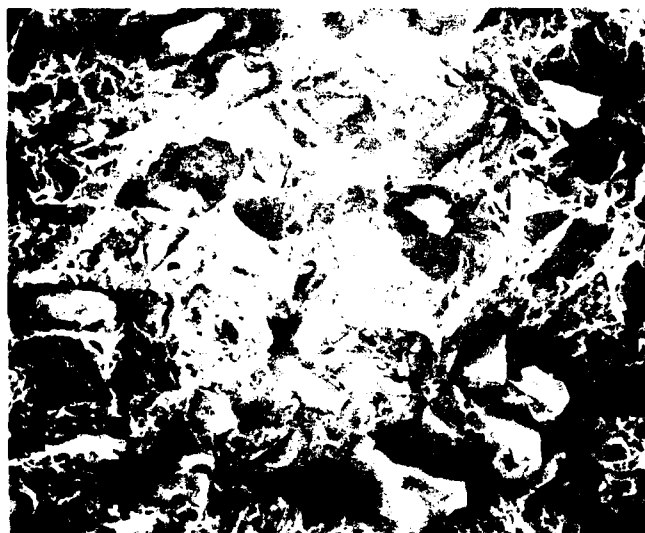


Figure 21. Ductility versus volume fraction of  $Al_2O_3$  particles in a number of aluminum alloy composites liquid forged into shape and heat treated to a T-4 condition.



(a)



(b)

Figure 22. Fracture surfaces of aluminum alloy composites containing  $\text{Al}_2\text{O}_3$  particles. (a) shows a 2014 alloy matrix containing 5 weight percent of  $5\mu\text{m}$  size particles at 1000X, (b) shows a 2014 alloy matrix containing 30 weight percent of  $14\mu\text{m}$  size particles at 100X.

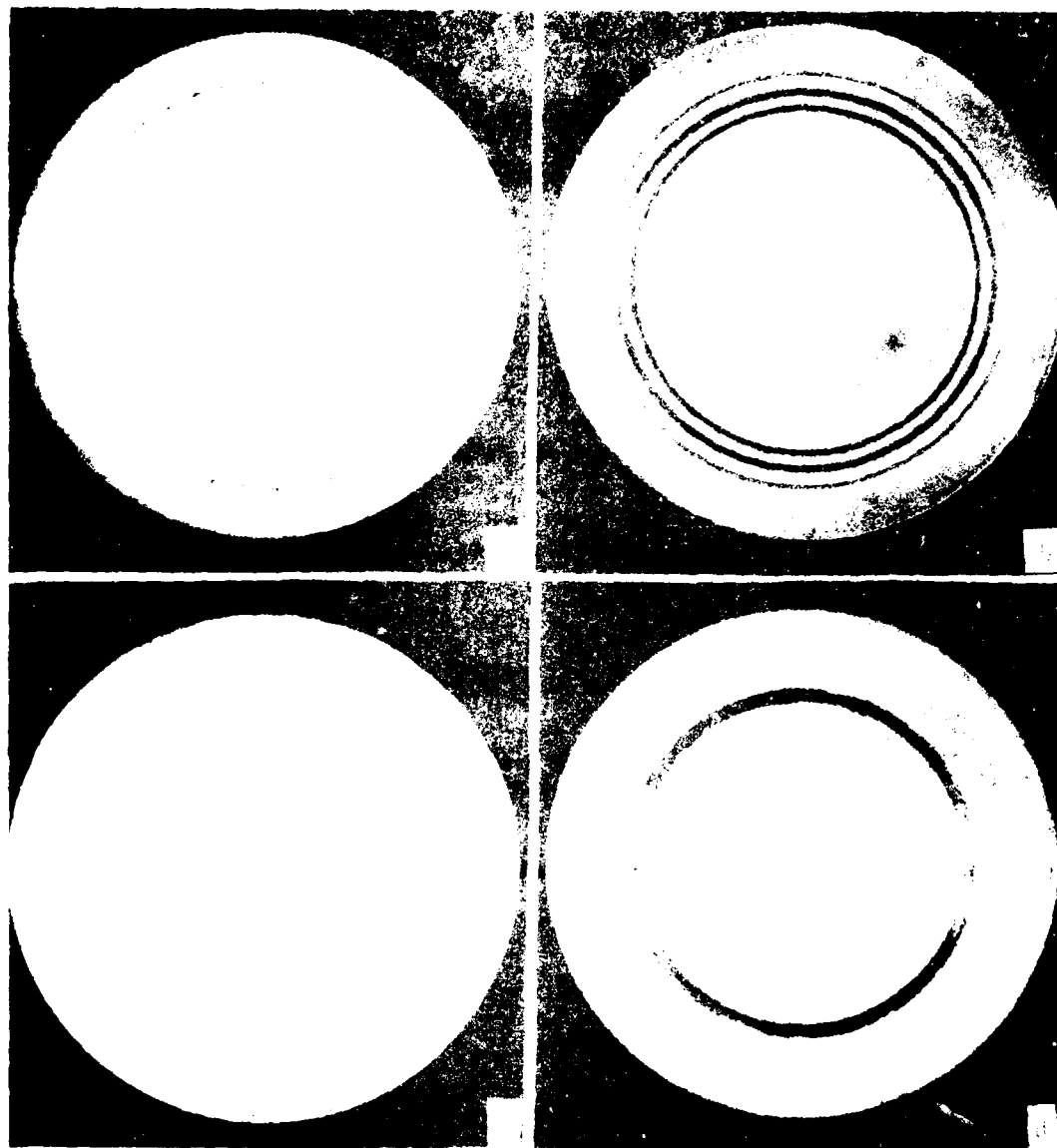


Figure 23. Photographs of cross-sections of (a) liquid forged matrix and (b) 2024 aluminum alloy matrix. (c) 2024 aluminum alloy matrix containing 20 wt. of  $Al_2O_3$  particles. (d) 2024 aluminum alloy matrix containing 20 wt. of 142 nm  $Al_2O_3$  particles.



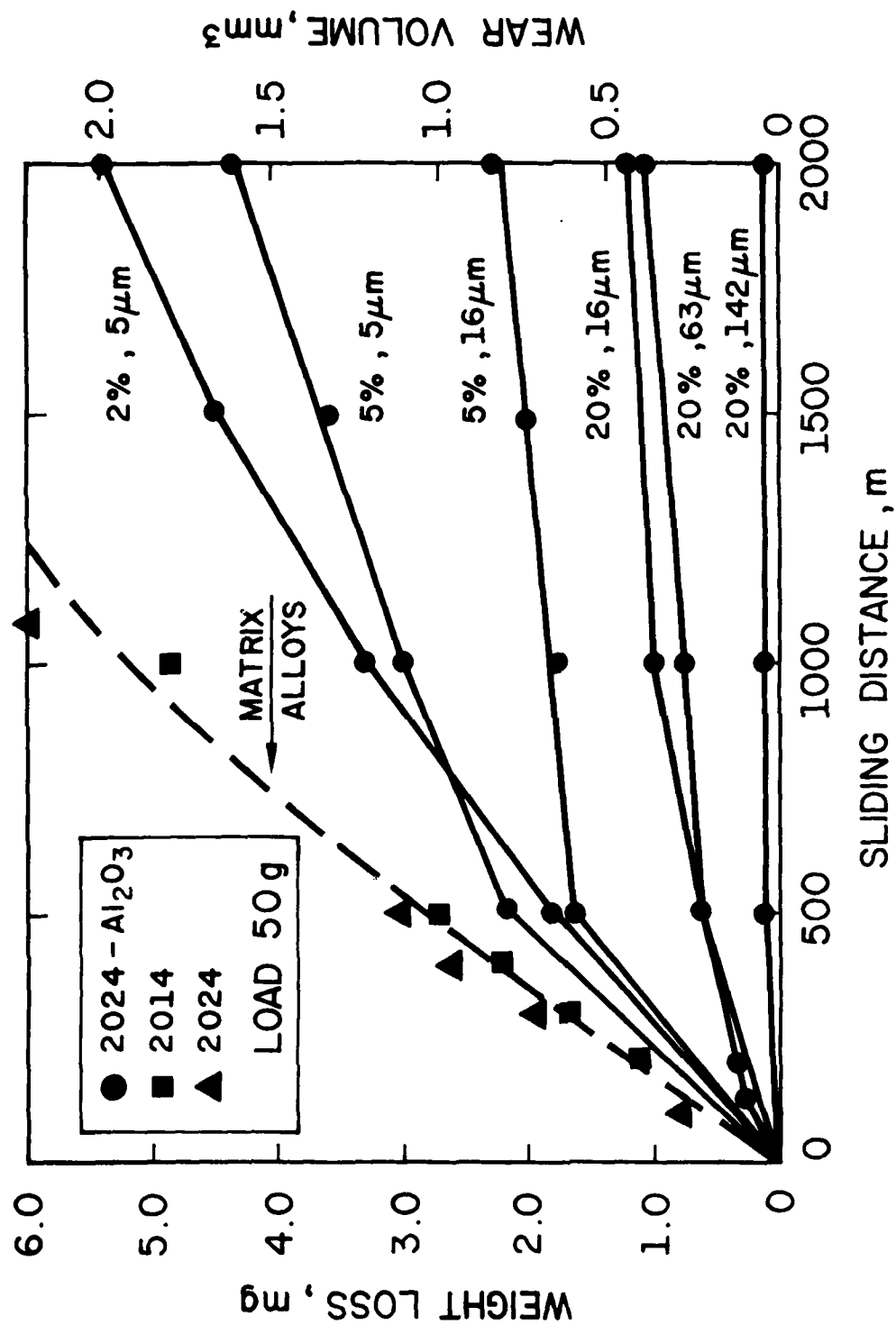


Figure 24. Weight loss versus sliding distance of aluminum matrix alloys 2014 and 2024 and composites of 2024 containing different weight percentages of four different size Al<sub>2</sub>O<sub>3</sub> particles. Applied load on the rider (pin) was 50 grams.

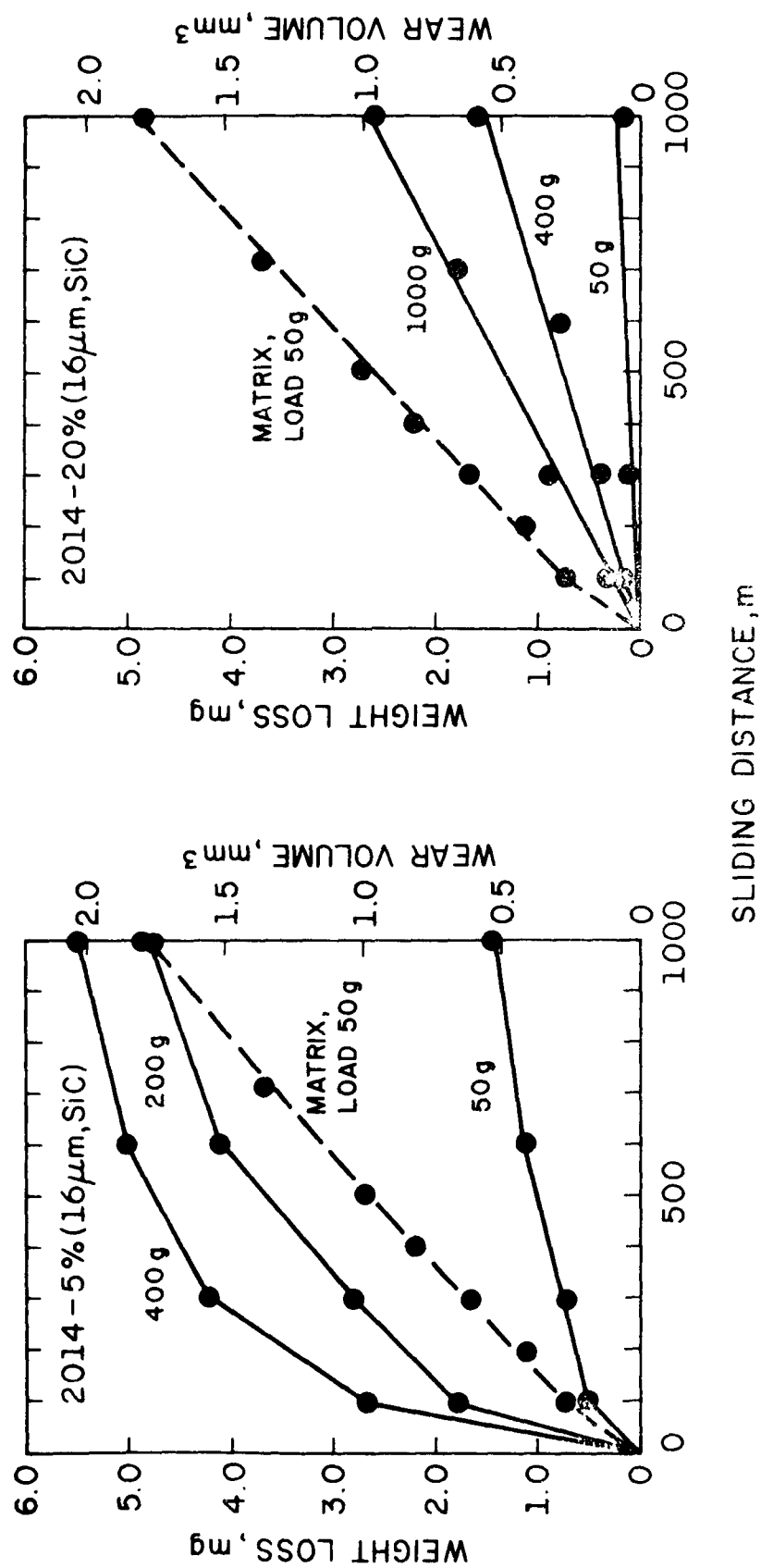


Figure 25. The effect of applied load on weight loss versus sliding distance of aluminum matrix alloy 2014 and composites of alloy 2014 containing 5 and 20 wt % of 15 $\mu$ m size SiC particles.

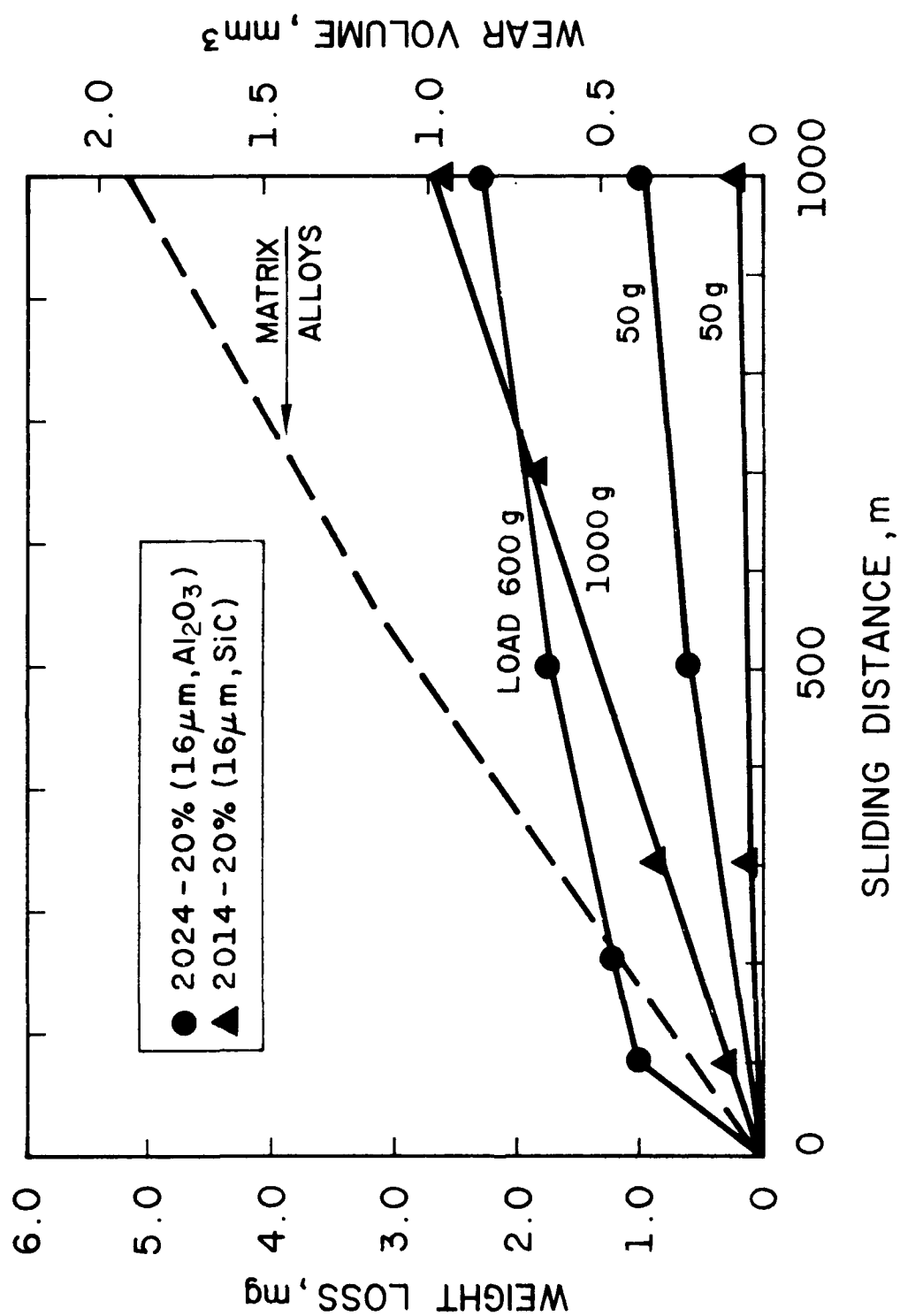


Figure 26. Comparison of the wear behavior of composites containing SiC and Al<sub>2</sub>O<sub>3</sub> particles.

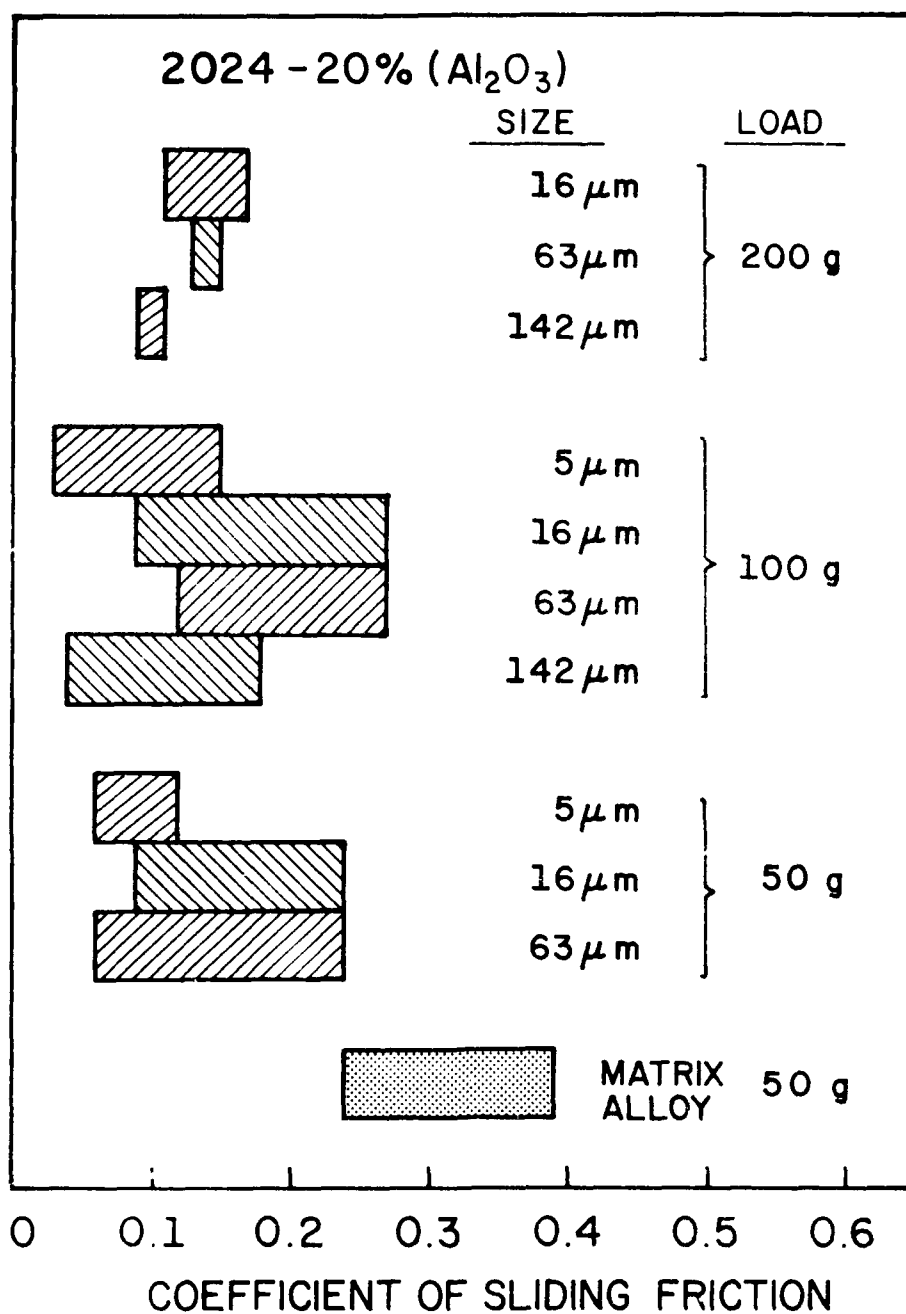


Figure 27. Average measured coefficient of sliding friction of aluminum matrix alloy 2024 and a composite of the alloy containing 20 wt% of different size  $\text{Al}_2\text{O}_3$  particles.

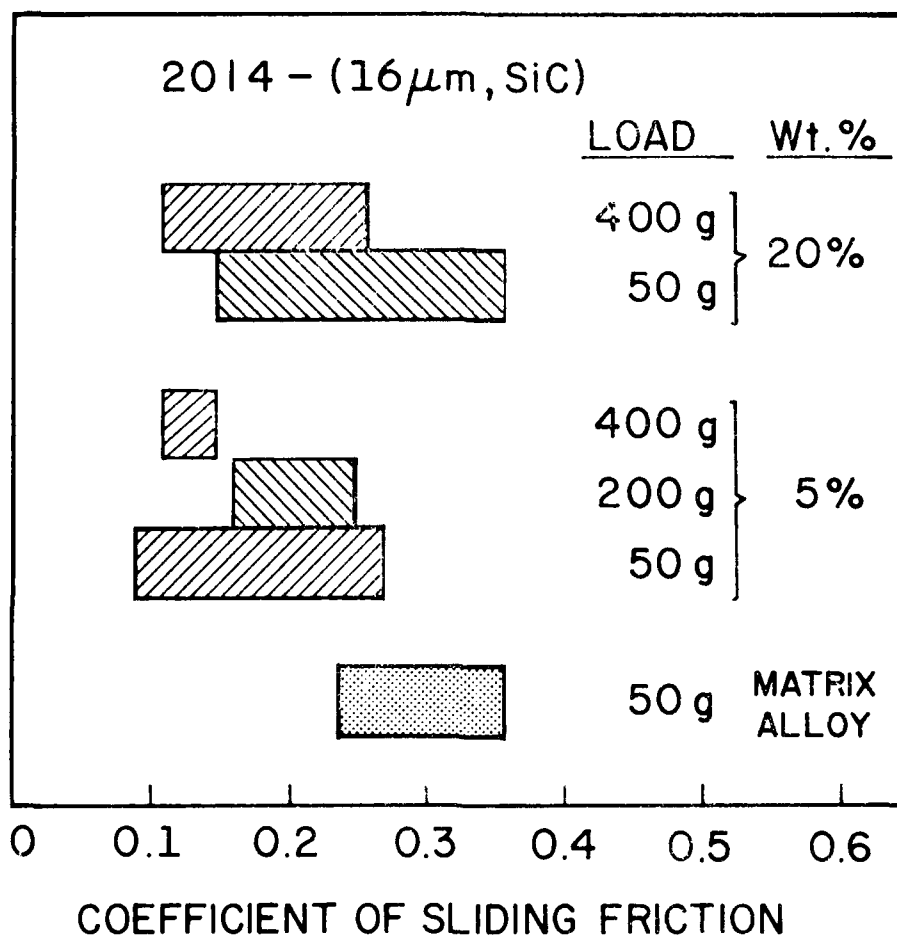


Figure 28. Average measured coefficient of sliding friction of aluminum matrix alloy 2014 and a composite of the alloy containing 5 and 20 wt% of 16 $\mu$ m size SiC particles.

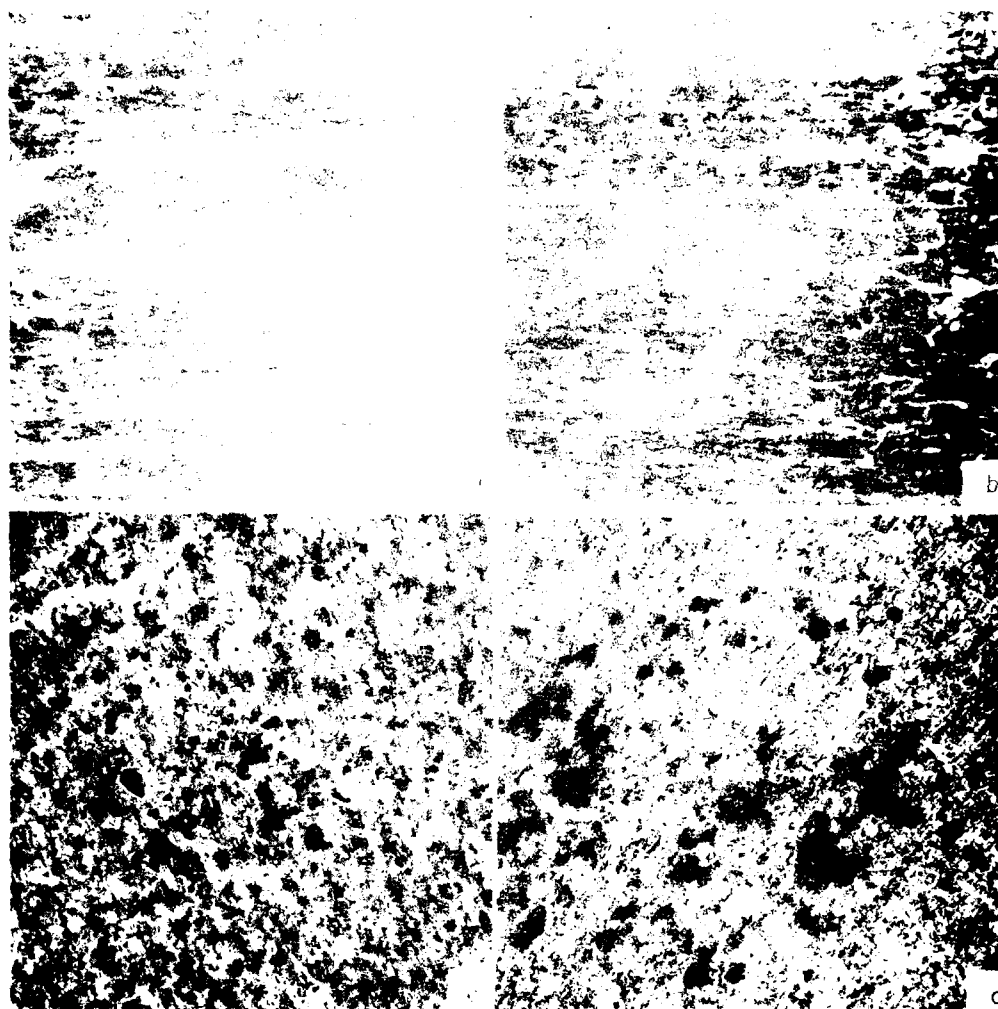


Figure 29. Microstructure of the wear track of aluminum alloy and aluminum alloy composites after 200 cycles with an applied load of 200 grams at 100x. (a) Aluminum alloy 2014, (b) aluminum alloy 2014 containing 5 wt% of 16µm  $Al_2O_3$  particles, (c) aluminum alloy 2014 containing 20 wt% of 16µm  $Al_2O_3$  particles and (d) aluminum alloy 2014 containing 20 wt% of 16µm SiC particles.



Figure 16. (b) and (d) show the steel ball bearing wear tracks in Figure 16

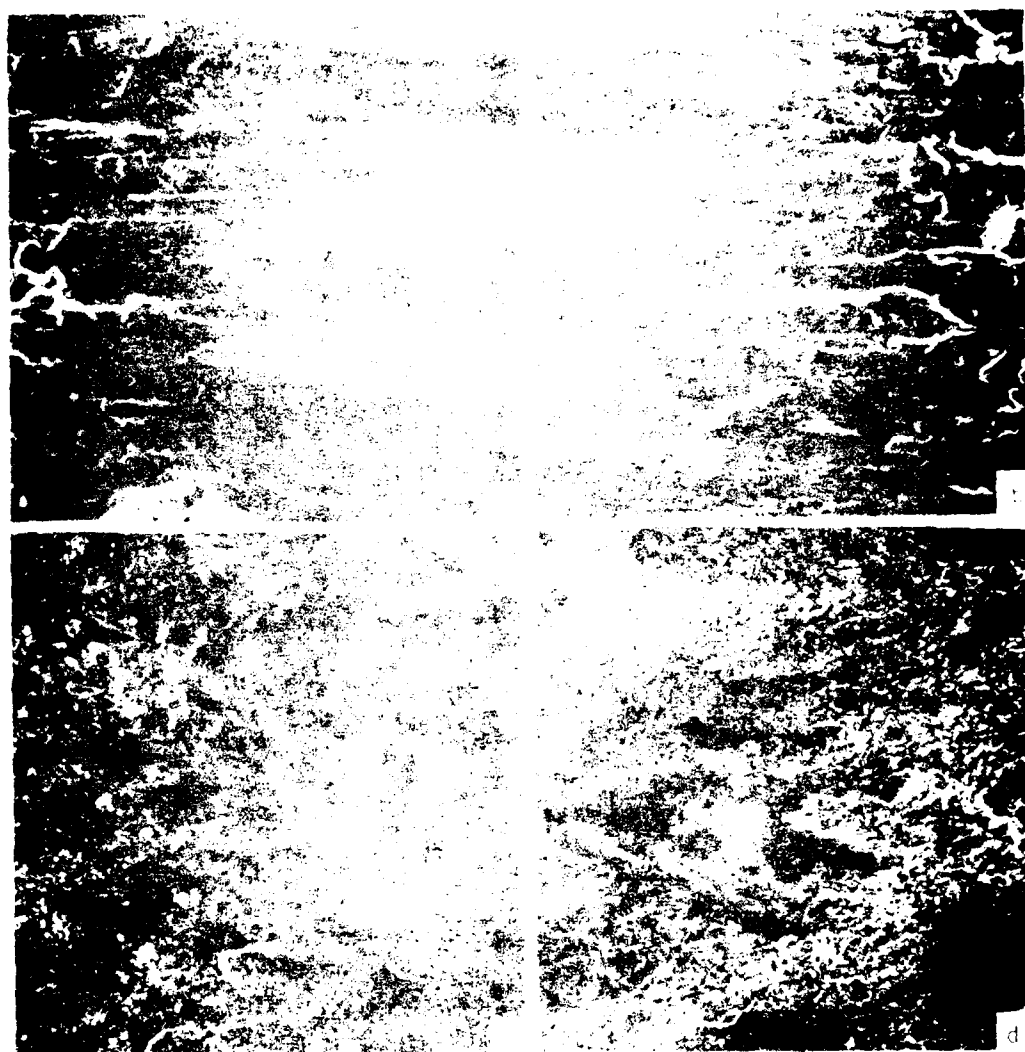


Figure 11. Micrographs of aluminum surfaces after 1000 hours of exposure to air. (a) and (b) are surfaces of grains at 1000 hours. (c) and (d) are surfaces of grains at 1000 hours. The aluminum surface was etched with 10%  $\text{Al}_2\text{O}_3$  peroxide solution. The surface contained 20% aluminum. The surface of aluminum peroxide was etched with 10%  $\text{Al}_2\text{O}_3$  peroxide solution.





Figure 32. Microstructures of the wear track of an aluminum alloy 2024 containing 20 wt% of 142 $\mu$ m size Al<sub>2</sub>O<sub>3</sub> particles at 100X. Sliding velocity and load were 10 cm/sec and 200 grams, respectively. (a), (b) and (c) show the microstructures after 15, 35 and 200 revolutions, respectively.

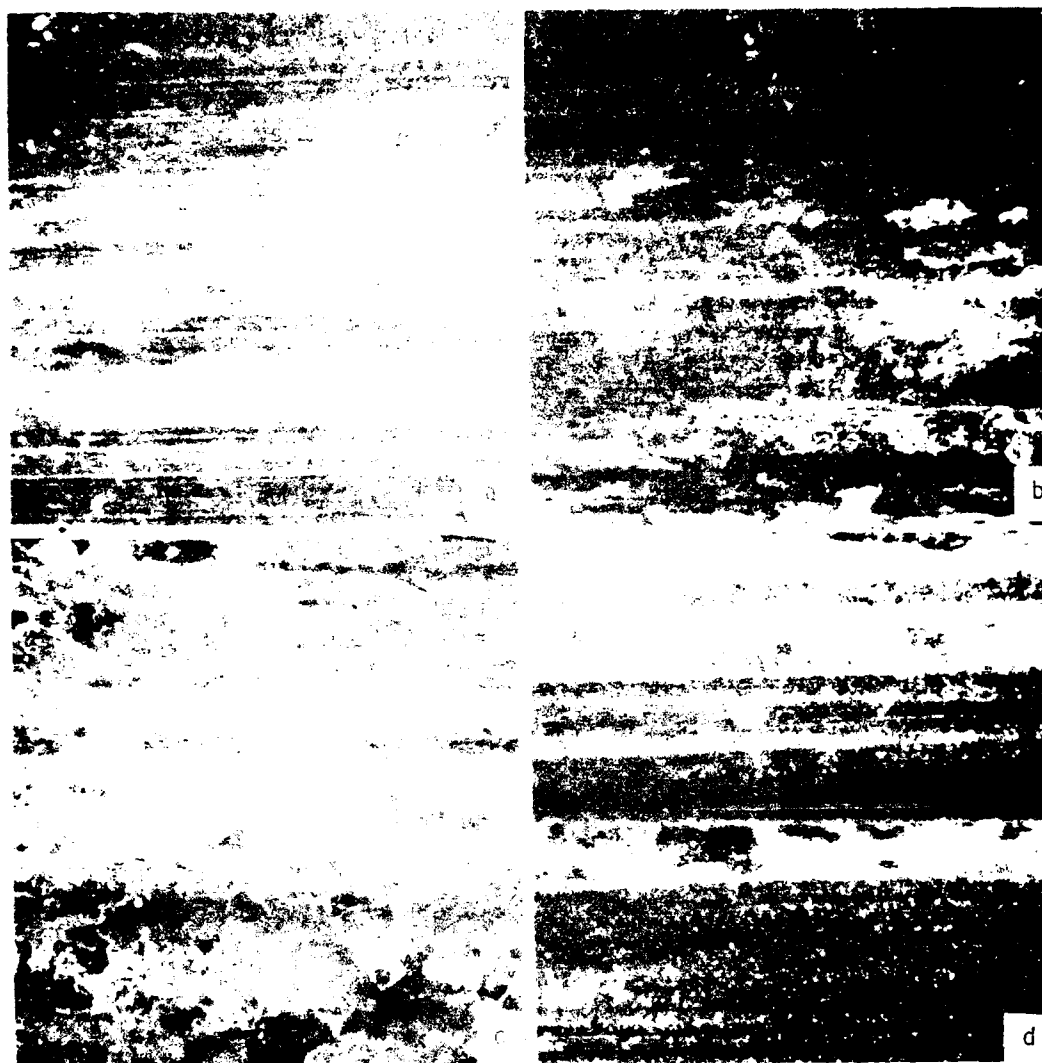


Figure 33. Microstructures of the wear tracks on both the aluminum alloy composites and the corresponding steel ball bearings at 200X. (a) and (c) show the aluminum alloy 2014 containing 20 wt% of 16μm size  $Al_2O_3$  particles and the corresponding pin, respectively; (b) and (d) show the aluminum alloy 2014 containing 20 wt% 16μm size SiC particles and the corresponding pin, respectively.



Figure 34. Low magnification views of the ball bearings shown in Figure 20 at 20X. (a) and (b) correspond to (c) and (d) in Figure 20, respectively.

# DISTRIBUTION LIST

No. of Copies	To
1	Office of the Under Secretary of Defense for Research and Engineering, The Pentagon, Washington, D. C. 20301
12	Commander, Defense Technical Information Center, Cameron Station, Building 5, 5010 Duke Street, Alexandria, Virginia 22314
1	Metals and Ceramics Information Center, Battelle Columbus Laboratories, 505 King Avenue, Columbus, Ohio 43201
	Deputy Chief of Staff for Research, Development, and Acquisition, Washington, D. C. 20310
1	ATTN: DAMA-ARZ
	Commander, Army Research Office, P. O. Box 12211, Research Triangle Park, North Carolina 27709
1	ATTN: Information Processing Office
	Commander, U. S. Army Materiel Development and Readiness Command, 5001 Eisenhower Avenue, Alexandria, Virginia 22333
1	ATTN: DRCLDC, Mr. R. Zentner
	Commander, U. S. Army Electronics Research and Development Command, Fort Monmouth, New Jersey 07703
1	ATTN: DELSD-L
1	DELS-D-E
	Commander, U. S. Army Armament Research and Development Command, Dover, New Jersey 07801
2	ATTN: Technical Library
1	DRDAR-SCM, Mr. J. D. Corrie
1	Plastics Technical Evaluation Center, PLASTEC, Harry E. Peibly, Jr., Director
	Commander, U. S. Army Natick Research and Development Command, Natick, Massachusetts 01760
1	ATTN: Technical Library
	Director, U. S. Army Ballistic Research Laboratory, Aberdeen Proving Ground, Maryland 21005
1	ATTN: DRDAR-TSB-S (STINFO)
	Commander, U. S. Army Satellite Communications Agency, Fort Monmouth, New Jersey 07703
1	ATTN: Technical Document Center

No. of Copies	To
	Commander, U. S. Army Tank-Automotive Research and Development Command, Warren, Michigan 48090
1	ATTN: DRDTA-RKA
2	DRDTA-UL, Technical Library
	Commander, White Sands Missile Range, New Mexico 88002
1	ATTN: STEWS-WS-VT
	Commander, Harry Diamond Laboratories, 2800 Powder Mill Road, Adelphi, Maryland 20783
1	ATTN: Technical Information Office
	Commander, Redstone Scientific Information Center, U. S. Army Missile Research and Development Command, Redstone Arsenal, Alabama 35809
1	ATTN: DRDMI-TB
	Commander, Watervliet Arsenal, Watervliet, New York 12189
1	ATTN: SARWV-RDT, Technical Information Services Office
	Commander, U. S. Army Foreign Science and Technology Center, 220 7th Street, N.E., Charlottesville, Virginia 22901
1	ATTN: Mr. Marley, Military Tech
	Director, Eustis Directorate, U. S. Army Air Mobility Research and Development Laboratory, Fort Eustis, Virginia 23604
1	ATTN: Mr. J. Robinson, DAVDL-E-MOS (AVRADCOM)
	U. S. Army Aviation Training Library, Fort Rucker, Alabama 36360
1	ATTN: Buildings 5906-5907
	Commander, USACDC Air Defense Agency, Fort Bliss, Texas 79916
1	ATTN: Technical Library
	Commander, U. S. Army Engineer School, Fort Belvoir, Virginia 22060
1	ATTN: Library
	Commander, U. S. Army Engineer Waterways Experiment Station, Vicksburg, Mississippi 39180
1	ATTN: Research Center Library
	Commander, U. S. Army Environmental Hygiene Agency, Edgewood Arsenal, Maryland 21010
1	ATTN: Chief, Library Branch
	Commander, U. S. Army Materiel Systems Analysis Activity, Aberdeen Proving Ground, Maryland 21005
1	ATTN: DRXSYP-MP, H. Cohen

No. of Copies	To
1	Naval Research Laboratory, Washington, D. C. 20375 ATTN: Dr. J. M. Krafft - Code 8430
1	Chief of Naval Research, Arlington, Virginia 22217 ATTN: Code 471
2	Air Force Materials Laboratory, Wright-Patterson Air Force Base, Ohio 45433 ATTN: AFML/MXE/E. Morrissey
1	AFML/LC
1	AFML/LLP/D. M. Forney, Jr.
1	AFML/MBC/Stanley Schulman
1	National Aeronautics and Space Administration, Washington, D. C. 20546 ATTN: Mr. B. G. Achhammer
1	Mr. G. C. Deutsch - Code RW
1	National Aeronautics and Space Administration, Marshall Space Flight Center, Huntsville, Alabama 35812 ATTN: R. J. Schwinghamer, EH01, Director, M&P Laboratory
1	Mr. W. A. Wilson, EH41, Building 4612
1	Air Force Flight Dynamics Laboratory, Wright-Patterson Air Force Base, Ohio 45433 ATTN: AFFDL (FBS), C. Wallace
1	AFFDL (FBEB), G. D. Sendeckyj
1	National Aeronautics and Space Administration, Langley Research Center, Hampton, Virginia 23365 ATTN: Mr. H. F. Hardrath, Mail Stop 188M
1	National Aeronautics and Space Administration, Lewis Research Center, 21000 Brookpark Road, Cleveland, Ohio 44135 ATTN: Dr. J. E. Srawley, Mail Stop 105-1
1	Mr. W. F. Brown, Jr.
1	National Bureau of Standards, U. S. Department of Commerce, Washington, D. C. 20234 ATTN: Mr. J. A. Bennett
1	Virginia Polytechnic Institute and State University, Dept. of Engineering Mechanics, 230 Norris Hall, Blacksburg, Virginia 24061 ATTN: Prof. R. M. Barker
1	Southwest Research Institute, 8500 Culebra Road, San Antonio, Texas 78284 ATTN: Mr. G. C. Grimes
1	Westinghouse Electric Company, Pittsburgh, Pennsylvania 15235 ATTN: Mr. E. T. Wessel, Research and Development Center

No. of  
Copies

To

- 
- |   |   |
|---|---|
| 1 | Mr. M. J. Manjoine, Westinghouse Research Laboratory, Churchill Boro,<br>Pittsburgh, Pennsylvania 15235   |
| 1 | Mr. William J. Walker, Air Force Office of Scientific Research,<br>1400 Wilson Boulevard, Arlington, Virginia 22209                                       |
| 1 | Mr. Elmer Wheeler, Airesearch Manufacturing Company, 402 S. 36th Street,<br>Phoenix, Arizona 85034  |
| 1 | Mr. Charles D. Roach, U. S. Army Scientific and Technical Information Team,<br>6000 Frankfurt/Main, I.G. Hochhaus, Room 750, West Germany (APO 09710, NY) |
| 1 | Dr. Robert S. Shane, Shane Associates Incorporated, 7821 Carrleigh Parkway,<br>Springfield, Virginia 22152  |
|   | Director, Army Materials and Mechanics Research Center,<br>Watertown, Massachusetts 02172   |
| 2 | ATTN: DRXMR-PL  |
| 1 | DRXMR-PR  |
| 1 | DRXMR-PD  |
| 1 | DRXMR-AP  |
| 3 | DRXMR-ER, Mr. R. Gagne  |

[illegible][illegible][illegible][illegible]



